

Unit 2b.2: Dynamical Diffraction **in *Methods in Materials Research* (John Wiley & Sons, 2000)**

Qun Shen

Cornell High Energy Synchrotron Source (CHESS)
and Department of Materials Science and Engineering
Cornell University, Ithaca, New York 14853

-
- I. Introduction
 - Application areas
 - Brief survey of literature
 - Scope of this unit
 - II. Basic Principles
 - Fundamental equations
 - Dispersion surface
 - Boundary conditions
 - Internal fields
 - III. Two-Beam Diffraction
 - Properties of dispersion surface
 - Special dynamical effects
 - Solution of dispersion equation
 - Diffracted intensities
 - Standing waves
 - IV. Multiple-Beam Diffraction
 - Basic concepts
 - NBEAM theory
 - Second-order Born approximation
 - Special multi-beam effects
 - Polarization density matrix
 - V. Grazing Angle Diffraction
 - Fresnel reflectivity
 - Evanescent wave
 - Multilayers and superlattices
 - Grazing incidence diffraction
 - Distorted-wave Born approximation
 - VI. Summary
 - VII. References
-

Unit 2b.2: Dynamical Diffraction

I. INTRODUCTION

Diffraction related techniques using x-rays, electrons or neutrons are widely used in materials science to provide basic structural information on crystalline matters. To describe a diffraction phenomenon, one has the choice of two theories: kinematic theory or dynamical theory.

Kinematic theory, described in the last Unit, assumes that each x-ray photon, electron, or neutron scatters only once before it is detected. This assumption is valid in most cases for x-rays and neutrons since their interactions with materials are relatively weak. The single scattering mechanism is also called the *first order Born approximation* or simply the *Born approximation* (Schiff, 1955; Jackson, 1975). As amply demonstrated in the last Unit, the kinematic diffraction theory can be applied to a vast majority of materials studies and is the most commonly used theory to describe x-ray or neutron diffraction from crystals that are imperfect.

There are, however, practical situations where the higher-order scattering or multiple scattering terms in the Born series become important and cannot be neglected. This, for example, is the case for electron diffraction from crystals, where an electron beam interacts strongly with electrons in a crystal. Multiple scattering can also be important in certain application areas of x-ray and neutron scattering, as described below. In all these cases the simplified kinematic theory is not sufficient to evaluate the diffraction processes and the more rigorous *dynamical theory* is needed where multiple scattering is taken into account.

Application Areas

Dynamical diffraction is the predominant phenomenon in almost all electron diffraction applications, such as low energy electron diffraction and reflection high-energy electron diffraction. For x-rays and neutrons areas of materials research that involve dynamical diffraction may include the following situations:

(1) **Strong Bragg reflections**: For Bragg reflections with large structure factors, the kinematic theory often overestimates the integrated intensities. This occurs for many real crystals such as minerals and even biological crystals such as proteins, since they are not ideally imperfect. The effect is usually called the *extinction* (Warren, 1969), which refers to the extra attenuation of the incident beam in the crystal due to the loss of intensity to the diffracted beam. Its characteristic length scale, *extinction length*, depends on the structure factor of the Bragg reflection being measured. One can further

categorize extinction effects into two types: *primary extinction*, which occurs within individual mosaic blocks in a mosaic crystal, and *secondary extinction*, that occurs for all mosaic blocks along the incident beam path. Primary extinction exists when the extinction length is shorter than the average size of mosaic blocks and secondary extinction occurs when the extinction length is less than the absorption length in the crystal.

(2) **Large nearly-perfect crystals and multilayers**: It is not uncommon in today's materials preparation and crystal growth laboratories that one has to deal with large nearly-perfect crystals. Often centimeter-sized perfect semiconductor crystals such as GaAs and Si are used as substrate materials and multilayers and superlattices are deposited using molecular-beam or chemical vapor epitaxy. Bulk crystal growers are also producing larger high quality crystals by advancing and perfecting various growth techniques. Characterizations of these large nearly-perfect crystals and multilayers by diffraction techniques often involve the use of dynamical theory simulations of the diffraction profiles and intensities. Crystal shape and its geometry with respect to the incident and the diffracted beams can also influence the diffraction pattern which can only be accounted for by dynamical diffraction.

(3) **Topographic studies of defects**: X-ray diffraction topography is a useful technique to study crystalline defects such as dislocations in large-grain nearly perfect crystals (Chikawa & Kuriyama, 1991; Klapper, 1996; Tanner, 1996). With this technique an extended highly collimated x-ray beam is incident on a specimen and an image of one or several strong Bragg reflected are recorded with high-resolution photographic films. Examination of the image can reveal μm sized crystal defects such as dislocations, growth front, fault lines, etc.. Because the strain field induced by a defect can extend far into the single crystal grain, the diffraction process is rather complex and a quantitative interpretation of a topographic image frequently requires the use of dynamical theory and its variation on distorted crystals developed by Takagi (1962, 1969) and Taupin (1964).

(4) **Internal-field-dependent diffraction phenomena**: Several diffraction techniques make use of the secondary excitations induced by the wave field inside a crystal under diffraction condition. These secondary signals may be x-ray fluorescence or secondary electrons such as Auger or photoelectrons. The intensities of these signals are directly proportional to the electric field strength at the atom position where the secondary signal is generated. The wave field strength inside the crystal is a sensitive function of the crystal orientation near a specular or a Bragg reflection and the dynamical theory is the only theory that provides the internal wave field amplitudes including the interference between the incident and the diffracted waves or the standing wave effect (Batterman, 1964). As a variation of the standing

wave effect, the secondary signals can be diffracted by crystal lattice and form standing wave like diffraction profiles. These include Kossel lines for x-ray fluorescence (Kossel, 1935) and Kikuchi lines for secondary electrons (Kikuchi, 1928). These effects can be interpreted as the optical reciprocity phenomena of the standing wave effect.

(5) **Multiple Bragg diffraction studies:** If a single crystal is oriented in such a way that more than one reciprocal nodes fall on the Ewald sphere of diffraction, a simultaneous multiple-beam diffraction would occur. These simultaneous reflections were first discovered by Renninger (1937) and are often called Renninger reflections or detour reflections (*umweganregung*). Although the angular positions of the simultaneous reflections can be predicted by simple geometric considerations in reciprocal space (Cole, Chambers & Dunn, 1962), a theoretical formalism that goes beyond the kinematic theory or the first order Born approximation is needed to describe the intensities of a multiple-beam diffraction (Colella, 1974). Because of the interference among the simultaneously excited Bragg beams, multiple-beam diffraction promises to be a practical solution to the phase problem in diffraction-based structural determination of crystalline materials, and there has been a great renewed interest in this research area (Shen, 1998; 1999a,b; Chang, et al. 1999).

(6) **Grazing-incidence diffraction:** In grazing incidence diffraction geometry, either the incident beam or the diffracted beam or both has an incident or exit angle, with respect to a well-defined surface, close to the critical angle of the diffracting crystal. Full treatment of the diffraction effects in grazing angle geometry involves Fresnel specular reflection and requires the concept of an evanescent wave that travels parallel to the surface and decays exponentially as a function of depth into the crystal. The dynamical theory is needed to describe the specular reflectivity and the evanescent wave related phenomena. Because of its surface sensitivity and adjustable probing depth, grazing incidence diffraction of x-rays and neutrons has evolved into an important technique for materials research and characterization.

Brief Survey of Literature

Dynamical diffraction theory of a plane wave by a perfect crystal was originated by Darwin (1914) and Ewald (1916), using two very different approaches. Since then the early development of the dynamical theory was primarily focused on the situations involving only an incident beam and one Bragg diffracted beam, the so-called two-beam case. Prins (1930) extended the Darwin's theory to take into account of absorption, and von Laue (1931) reformulated Ewald's approach and formed the backbone of the modern-day dynamical theory. Reviews and extensions of the theory have been

given by Zachariasen (1945), James (1950), Kato (1952), Warren (1969), and Authier (1970). A comprehensive review of the Ewald-von Laue theory has been provided by Batterman and Cole in their seminal article in *Review of Modern Physics* (1964). More recent reviews can be found in Kato (1974), Cowley (1975) and Pinsker (1978). Updated and concise summaries of the two-beam dynamical theory have been given recently by Authier (1992, 1996). A historical survey of the early development of the dynamical theory was given in Pinsker (1978).

Contemporary topics in dynamical theory are mainly focused in the following four areas: multiple-beam diffraction, grazing incidence diffraction, internal fields and standing waves, and special x-ray optics. These modern developments are largely driven by recent interests in rapidly emerging fields such as synchrotron radiation, x-ray crystallography, surface science, and semiconductor research.

Dynamical theory of x-rays for multiple-beam diffraction, with two or more Bragg reflections excited simultaneously, was considered by Penning (1967), Ewald and Heno (1968). However, very little progress was made until Colella (1974) developed a computational algorithm that made multiple-beam x-ray diffraction simulations more tractable. Recent interests in its applications to measure the phases of structure factors (Colella, 1974; Post, 1977; Chang, 1982; Chapman, Yoder & Colella, 1981) have made multiple-beam diffraction an active area of research in dynamical theory and experiments. Approximate theories of multiple-beam diffraction have been developed by Juretschke (1982, 1984, 1986), Hoier & Marthinsen (1983), Hummer & Billy (1986), Shen (1986, 1999b, 2000), and Thorkildsen (1987). Reviews on multiple-beam diffraction have been given by Chang (1984, 1992, 1998), Colella (1995), and Weckert & Hummer (1997).

Since the pioneer experiment by Marra, Eisenberger, and Cho (1979), there has been an enormous increase in the development and the use of grazing incidence x-ray diffraction to study surfaces and interfaces of solids. Dynamical theory for the grazing angle geometry was soon developed (Afanasev & Melkonyan, 1983; Aleksandrov et al. 1984) and its experimental verifications were given by Cowan et al. (1986), Durbin and Gog (1989), and Jach et al. (1989). Meanwhile, a semi-kinematic theory called Distorted Wave Born Approximation was used by Vineyard (1982) and by Dietrich and Wagner (1983, 1984). This theory was further developed by Dosch et al. (1986) and Sinha et al. (1988), and has become widely utilized in glancing-incidence x-ray scattering studies of surface and near-surface structures. The theory has also been extended to explain standing-wave enhanced and non-specular scattering in multilayer structures (Kortright, 1987), and

to include phase-sensitive scattering in diffraction from bulk crystals (Shen, 1999b).

Direct experimental proof of the x-ray standing wave effect was first achieved by Batterman (1964) by observing x-ray fluorescence profiles while the diffracting crystal is rotated through a Bragg reflection. Earlier works were mainly on locating impurity atoms in bulk semiconductor materials (Batterman, 1969; Golovchenko et al. 1974; Anderson et al. 1976), but more recent research activities have been on determinations of atom locations and distributions in overlayers above crystal surfaces (Golovchenko et al. 1982; Funke & Materlik, 1985; Durbin et al. 1986; Patel et al. 1987; Bedzyk et al. 1989), in synthetic multilayers (Barbee & Warburton, 1984; Kortright & Fischer-Colbrie, 1987), in long-period overlayers (Bedzyk et al. 1988; Wang et al. 1992), and in electrochemical solutions (Bedzyk et al. 1986). Recent reviews on x-ray standing waves have been given by Patel (1996) and Lagomarsino (1996).

Rapid increase in synchrotron-radiation-based materials research in recent years has spurred new developments in x-ray optics (Batterman & Bilderback, 1991; Hart, 1996). This is especially true in the areas of x-ray wave guides for producing sub-micron sized beams (Bilderback, 1994; Feng et al. 1995; Golovchenko et al. 1997), and x-ray phase plates and polarization analyzers used for studies on magnetic materials (Golovchenko et al. 1986; Mills, 1988; Belyakov & Dmitrienko, 1989; Hirano et al., 1991; Batterman, 1992; Shen & Finkelstein, 1992; Giles et al. 1994; Yahnke et al. 1994; Shastri et al. 1995). Recent reviews on polarization x-ray optics have been given by Hirano, Ishikawa and Kikuta (1995), Shen (1996), and Malgrange (1996).

An excellent collection of articles on these and other current topics in dynamical diffraction can be found in *X-ray and Neutron Dynamical Diffraction Theory and Applications*, edited by Authier, Lagomarsino and Tanner (1996).

Scope of This Unit

Given the wide range of topics in dynamical diffraction, the main purpose of this Unit is not to cover every detail but to provide readers with an overview of the basic concepts, formalisms, and applications in this field. Special attention is paid to the difference between the more familiar kinematic theory and the more complex dynamical approach. Although the basic dynamical theory is the same for x-rays, electrons, and neutrons, we will focus mainly on x-rays since many of the original terminology was founded in x-ray dynamical diffraction. The formalism for x-rays is also more complex and thus more complete because of the vector-field nature of an electromagnetic wave. For reviews on dynamical diffraction of electrons and neutrons, we refer the readers

to an excellent textbook by Cowley (1975), the 2nd edition of *International Tables for Crystallography*, vol.B, and a recent article by Schlenker and Guigay (1996).

We will start in Section II with the fundamental equations and concepts in dynamical diffraction theory, derived from classical electrodynamics. Then in Section III we move onto the widely-used two-beam approximation essentially following the description of Batterman and Cole (1964). The two-beam theory deals with only the incident beam and one strongly diffracted Bragg beam, and the multiple scattering between the two beams. Multiple scattering due to other Bragg reflections are ignored. This theory provides many basic concepts in dynamical diffraction, and is very useful in visualizing the unique physical phenomena in dynamical scattering.

A full multiple-beam dynamical theory, developed by Colella (1974), takes into account all multiple scattering effects and surface geometries and gives the most complete description of the diffraction processes in a perfect crystal by x-rays, electrons or neutrons. An outline of this theory is summarized in Section IV. Also included in this Section is an approximate formalism, given by Shen (1986), based on second-order Born approximations. This theory takes into account only double scattering in a multiple scattering regime yet provides a useful picture on the physics of multiple-beam interactions. Finally, an approximate yet more accurate multiple-beam theory (Shen, 1999b) based on an expanded distorted-wave approximation is presented, which can provide accurate accounts of three-beam interference profiles in the so-called reference-beam diffraction geometry (Shen, 1998).

In Section V the main results for grazing-incidence diffraction are described using the dynamical treatment. Of particular importance is the concept of evanescent waves and its applications. Also described in Section V is a so-called Distorted-wave Born approximation, which uses the dynamical theory to evaluate specular reflections but treats the surface diffraction and scattering within the kinematic regime. This approximate theory is useful in structural studies of thin films and multilayered heterostructures.

Finally, because of its limited space, a few topics are not covered in this article. One of these omitted topics is the theory by Takagi and Taupin for distorted perfect crystals. We refer the readers to the original articles (Takagi, 1962, 1969; Taupin, 1964) and recent publications by Bartels, Hornstra and Lobeek (1986) and by Authier (1996)

II. BASIC PRINCIPLES

There are two approaches to the dynamical theory. One is based on the works by Darwin (1914) and by Prins

(1930). This method first finds the Fresnel reflectance and transmittance for a single layer of atomic plane and then evaluates the total wave fields for a set of parallel atomic planes. The diffracted waves are obtained by solving a set of difference equations similar to the ones used in classical optics for a series of parallel slabs or optical filters. Although it had not been widely used for quite a long time due to its computational complexity, the Darwin's approach has gained more attention in recent years to evaluate reflectivity for multilayers and superlattices (Durbin & Follis, 1995), for crystal truncation effects (Caticha, 1994), and for quasicrystals (Chung & Durbin, 1995)

The other approach, developed by Ewald (1917) and von Laue (1931), treats the wave propagation in a periodic medium as an eigenvalue problem and use the boundary conditions to obtain Bragg reflected intensities. We will follow the Ewald-von Laue approach since many of the fundamental concepts in dynamical diffraction can be visualized more naturally by this approach and it can be easily extended to situations involving more than two beams.

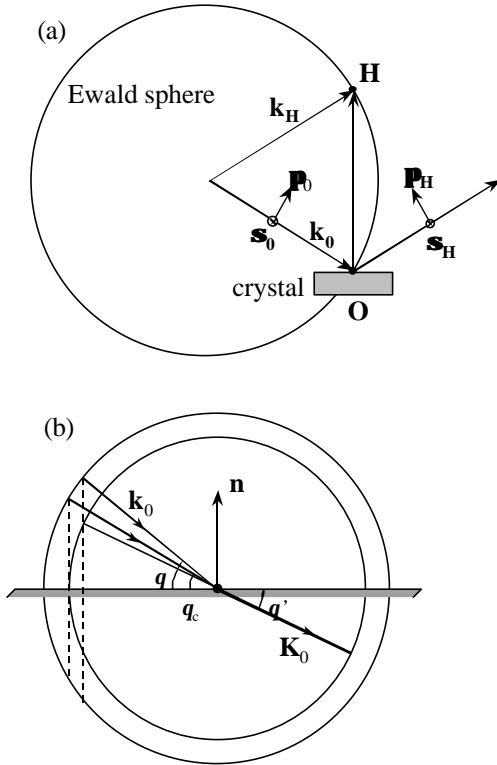


Figure 1: (a) Ewald sphere construction in kinematic theory and polarization vectors of the incident and the diffracted beams. (b) Dispersion surface in dynamical theory for a one-beam case and boundary conditions for total external reflection.

The mathematical forms for the diffracted intensities from general absorbing crystals appear to be rather complicated in the early literature of dynamical theory (for two-beams). The main reason for these complicated forms is the necessity to separate out the real and imaginary parts in dealing with complex wavevectors and wave field amplitudes before the times of computers and powerful calculators. In today's world these complicated equations are not necessary and numerical calculations with complex variables can be easily performed on a modern computer. Therefore in this article all final intensity equations are given in such compact forms that involve complex numbers and in author's view are best suited for today's computer calculations. These simpler forms also allow readers to gain physical insights rather than be overwhelmed by tedious mathematical notations.

Fundamental Equations

The starting point in the Ewald-von Laue approach of the dynamical theory is that the dielectric function $\mathbf{e}(\mathbf{r})$ in a crystalline material is a periodic function in space and therefore can be expanded in a Fourier series:

$$\mathbf{e}(\mathbf{r}) = \mathbf{e}_0 + \mathbf{de}(\mathbf{r}), \quad \text{with } \mathbf{de}(\mathbf{r}) = -\Gamma \sum_H F_H e^{-i\mathbf{H}\cdot\mathbf{r}}, \quad (1)$$

where $\Gamma = r_e \lambda^2 / (\pi V_c)$, $r_e = 2.818 \times 10^{-5} \text{ \AA}$ is the classical radius of an electron, λ the x-ray wavelength, V_c the unit cell volume, and $-\Gamma F_H$ is the coefficient of the \mathbf{H} Fourier component with F_H being the structure factor. All of the Fourier coefficients are on the order 10^{-5} to 10^{-6} or smaller at x-ray wavelengths, $\mathbf{de}(\mathbf{r}) \ll \mathbf{e}_0 = 1$, and the dielectric function is only slightly less than unity.

We further assume that a monochromatic plane wave is incident on a crystal, and the dielectric response is of the same wave frequency (elastic response). From Maxwell's equations and neglecting the magnetic interactions ($\mu=1$), we obtain the following equation for the electric field \mathbf{E} and the displacement vector \mathbf{D} :

$$(\nabla^2 + k_0^2) \mathbf{D} = -\nabla \times \nabla \times (\mathbf{D} - \mathbf{e}_0 \mathbf{E}),$$

where \mathbf{k}_0 is the wavevector of the monochromatic wave in vacuum, $k_0 = |\mathbf{k}_0| = 2\pi/\lambda$. For treatment involving magnetic interactions we refer to the publication by Durbin (1987). Assuming an isotropic relation between $\mathbf{D}(\mathbf{r})$ and $\mathbf{E}(\mathbf{r})$, $\mathbf{D}(\mathbf{r}) = \mathbf{e}(\mathbf{r})\mathbf{E}(\mathbf{r})$, and $\mathbf{de}(\mathbf{r}) \ll \mathbf{e}_0$, we have

$$(\nabla^2 + k_0^2) \mathbf{D} = -\nabla \times \nabla \times (\mathbf{deD}). \quad (2)$$

We now use the periodic condition Eq.(1) and substitute the wave field \mathbf{D} in Eq.(2) by a series of Bloch waves with wavevectors $\mathbf{K}_H = \mathbf{K}_0 + \mathbf{H}$,

$$\mathbf{D}(\mathbf{r}) = \sum_{\mathbf{H}} \mathbf{D}_{\mathbf{H}} e^{-i\mathbf{K}_{\mathbf{H}} \cdot \mathbf{r}},$$

where \mathbf{H} is a reciprocal space vector of the crystal. For every Fourier component (Bloch wave) \mathbf{H} we arrive at the following equation:

$$\left[(1 - \Gamma F_0) k_0^2 - K_{\mathbf{H}}^2 \right] \mathbf{D}_{\mathbf{H}} = -\Gamma \sum_{\mathbf{G} \neq \mathbf{H}} F_{\mathbf{H}-\mathbf{G}} \mathbf{K}_{\mathbf{H}} \times (\mathbf{K}_{\mathbf{H}} \times \mathbf{D}_{\mathbf{G}}), \quad (3)$$

where the terms involving Γ^2 have been neglected and $\mathbf{K}_{\mathbf{H}} \cdot \mathbf{D}_{\mathbf{H}}$ are set to zero because of the transverse wave nature of the electromagnetic radiation. Eq.(3) forms a set of fundamental equations for the dynamical theory of x-ray diffraction. Similar equations for electrons and neutrons can be found in the literature (e.g. Cowley, 1975).

Dispersion Surface

A solution to the eigenvalue equation Eq.(3) gives rise to all the possible wavevectors $\mathbf{K}_{\mathbf{H}}$ and wave field amplitude ratios inside a diffracting crystal. The loci of the possible wavevectors form a multiple-sheets three-dimensional surface in reciprocal space and this surface is called the *dispersion surface*, as given by Ewald (1917).

The introduction of the dispersion surface is the most significant difference between the kinematic theory and the dynamical theory. Here instead of a single Ewald sphere (Fig.1a), we have a continuous distribution of "Ewald spheres" with their centers located on the dispersion surface, giving rise to all possible traveling wavevectors inside the crystal.

As an example, we assume that the crystal orientation is far from any Bragg reflections, and thus only one beam, the incident beam \mathbf{K}_0 , would exist in the crystal. For this "one-beam" case, Eq.(3) becomes:

$$\left[(1 - \Gamma F_0) k_0^2 - K_0^2 \right] \mathbf{D}_0 = 0.$$

Thus we have

$$K_0 = k_0 / (1 + \Gamma F_0)^{1/2} = k_0 (1 - \Gamma F_0 / 2), \quad (4)$$

which shows that the wavevector \mathbf{K}_0 inside the crystal is slightly shorter than that in vacuum as a result of the average *index of refraction*, $n = 1 - \Gamma F_0 / 2$, where F_0' is the real part of F_0 and is related to the average density r_0 by

$$r_0 = \frac{\rho \Gamma F_0' \epsilon}{r_e I^2}. \quad (5a)$$

In the case of absorbing crystals, \mathbf{K}_0 and F_0 are complex variables and the imaginary part F_0'' of F_0 is related to the average *linear absorption coefficient* μ_0 by

$$m_0 = k_0 \Gamma F_0'' = 2\rho \Gamma F_0'' / I. \quad (5b)$$

Eq.(4) shows that the dispersion surface in the one-beam case is a refraction-corrected sphere centered around the origin in reciprocal space, as shown in Fig.1(b).

Boundary Conditions

Once Eq.(3) is solved and all possible waves inside the crystal are obtained, the necessary connections between the wave fields inside and outside the crystal is made through the *boundary conditions*. There are two types of boundary conditions in classical electrodynamics (Jackson, 1975). One states that the tangential components of the wavevectors have to be equal on both sides of an interface (Snell's law):

$$\mathbf{k}_t = \mathbf{K}_t. \quad (6)$$

Throughout this article we use the convention that outside vacuum wavevectors are denoted by \mathbf{k} and internal wavevectors are denoted by \mathbf{K} , and the subscript t stands for the tangential component of the vector.

To illustrate this point, we again consider the simple one-beam case as shown in Fig.1(b). Suppose that an x-ray beam \mathbf{k}_0 with an angle \mathbf{q} is incident on a surface with \mathbf{n} being its surface normal. To locate the proper internal wavevector \mathbf{K}_0 , we follow along \mathbf{n} to find its intersection with the dispersion surface, in this case the sphere with its radius defined by Eq.(4). However, we see immediately that this is possible only if \mathbf{q} is greater than a certain incident angle \mathbf{q}_c , which is the *critical angle* of the material. From Fig.1(b) we can easily obtain that $\cos \mathbf{q}_c = K_0 / k_0$, or for small angles, $\mathbf{q}_c = (\Gamma F_0)^{1/2}$. Below \mathbf{q}_c no traveling wave solutions are possible and thus total external reflection occurs.

The second set of boundary conditions states that the tangential components of the electric and magnetic field vectors, \mathbf{E} and $\mathbf{H} = \hat{\mathbf{k}} \times \mathbf{E}$, ($\hat{\mathbf{k}}$ is a unit vector along the propagation direction), are continuous across the boundary. In dynamical theory literature, the eigenequations for dispersion surfaces are expressed in terms of either electric field vector \mathbf{E} or electric displacement vector \mathbf{D} . These two choices are equivalent since in both cases a small longitudinal component on the order of ΓF_0 in the \mathbf{E} -field vector is ignored for its inclusion only contributes a term of Γ^2 in the dispersion equation. Thus \mathbf{E} and \mathbf{D} are interchangeable under this assumption and the boundary conditions can be expressed as the following:

$$\mathbf{D}_t^{in} = \mathbf{D}_t^{out}, \quad (7a)$$

$$(\hat{\mathbf{k}} \cdot \mathbf{D}^{in})_t = (\hat{\mathbf{K}} \cdot \mathbf{D}^{out})_t. \quad (7b)$$

In dynamical diffraction, the boundary condition Eq.6 or the Snell's law selects which points are excited on the dispersion surface or which waves actually exist inside the crystal, for a given incident condition. The conditions Eqs.7(a) & 7(b) on the field vectors are then used to evaluate the actual internal field amplitudes and the diffracted wave intensities outside the crystal.

Depending on number of beams included in the dispersion equation (3) and the diffraction geometry of the crystal, dynamical theory covers a wide-range of specific topics. In certain cases, the existence of some beams can be predetermined based on the physical law of energy conservation. In these cases only Eq.(7a) is needed for the field boundary condition. Such is the case of conventional two-beam diffraction as discussed in the next Section. However, both sets of conditions in Eq.(7) are needed for general multiple-beam cases and for grazing angle geometry.

Internal Fields

One of the important applications of the dynamical theory is to evaluate the wavefields *inside* the diffracting crystal, in addition to the *external* diffracted intensities. Depending on the diffraction geometry, an internal field can be a periodic standing wave as in the case of a Bragg diffraction, or an exponentially decayed evanescent wave as in the case of a specular reflection, or a combination of the two. Although no detectors *per se* can be put inside a crystal, the internal field effects can be observed through one of the following two ways.

The first is to detect secondary signals produced by an internal field, which include x-ray fluorescence, Auger electrons, and photoelectrons. These inelastic secondary signals are directly proportional to the internal field intensity and are incoherent with respect to the internal field. Examples of this effect include the standard x-ray standing wave techniques, and depth-sensitive x-ray fluorescence measurements under total external reflection.

The other way is to measure the elastic scattering of an internal field. In most cases, including the standing wave case, an internal field is a traveling wave along a certain direction, and therefore can be scattered by atoms inside the crystal. This is a coherent process and the scattering contributions are added on the level of amplitudes instead of intensities. An example of this effect is the diffuse scattering of an evanescent wave, in studies of surface or near-surface structures.

III. TWO-BEAM DIFFRACTION

In the two-beam approximation, we assume only one Bragg diffracted wave \mathbf{K}_H is important in the crystal, in

addition to the incident wave \mathbf{K}_0 . Then Eq.(3) reduces to the following two coupled vector equations:

$$\begin{cases} [(1-\Gamma F_0)k_0^2 - K_0^2] \mathbf{D}_0 = -\Gamma F_H \mathbf{K}_0 \times (\mathbf{K}_0 \times \mathbf{D}_H) \\ [(1-\Gamma F_0)k_0^2 - K_H^2] \mathbf{D}_H = -\Gamma F_H \mathbf{K}_H \times (\mathbf{K}_H \times \mathbf{D}_0) \end{cases} \quad (8)$$

The wavevectors \mathbf{K}_0 and \mathbf{K}_H define a plane which is usually called the scattering plane. Using a coordinate system shown in Figure 1(a), we can decompose the wavefield amplitudes into \mathbf{s} and \mathbf{p} polarization directions, and the equations for the two polarization states decouple and can be solved separately:

$$\begin{cases} [(1-\Gamma F_0)k_0^2 - K_0^2] D_{0s,p} - k_0^2 \Gamma F_H P D_{Hs,p} = 0 \\ -k_0^2 \Gamma F_H P D_{0s,p} + [(1-\Gamma F_0)k_0^2 - K_H^2] D_{Hs,p} = 0 \end{cases} \quad (9)$$

where $P = \mathbf{s}_H \cdot \mathbf{s}_0 = 1$ for \mathbf{s} polarization and $P = \mathbf{p}_H \cdot \mathbf{p}_0 = \cos(2\theta_B)$ for \mathbf{p} polarization, with θ_B being the Bragg angle. To seek nontrivial solutions, we set the determinant of Eq.(9) to zero and solve for K_0 :

$$\begin{vmatrix} (1-\Gamma F_0)k_0^2 - K_0^2 & -k_0^2 \Gamma F_H P \\ -k_0^2 \Gamma F_H P & (1-\Gamma F_0)k_0^2 - K_H^2 \end{vmatrix} = 0, \quad (10)$$

where K_H^2 is related to \mathbf{K}_0 through the Bragg's law, $K_H^2 = |\mathbf{K}_0 + \mathbf{H}|^2$. Solution of Eq.(10) defines the possible wavevectors in the crystal and gives rise to the dispersion surface in the two-beam case.

Properties of Dispersion Surface

To visualize what the dispersion surface looks like in the two-beam case, we define two parameters \mathbf{x}_0 and \mathbf{x}_H , as described in James (1950) and Batterman & Cole (1964):

$$\begin{aligned} \mathbf{x}_0 &\equiv [K_0^2 - (1-\Gamma F_0)k_0^2] / 2k_0 = K_0 - k_0(1-\Gamma F_0/2) \\ \mathbf{x}_H &\equiv [K_H^2 - (1-\Gamma F_0)k_0^2] / 2k_0 = K_H - k_0(1-\Gamma F_0/2) \end{aligned}$$

These parameters represent the deviations of the wavevectors inside the crystal from the average refraction-corrected values given by Eq.(4). It also shows that in general the refraction corrections for the internal incident and diffracted waves are different. Using these deviation parameters, the dispersion equation Eq.(10) becomes

$$\mathbf{x}_0 \mathbf{x}_H = \frac{1}{4} k_0^2 \Gamma^2 P^2 F_H F_H. \quad (11)$$

(1) **Hyperboloid sheets:** Since the right-hand side is a constant for a given Bragg reflection, the dispersion

surface given by Eq.(11) represents two sheets of hyperboloids in reciprocal space, for each polarization state P , as shown in Figure 2(a). The hyperboloids have their diameter point, Q , located around what would be the center of the Ewald sphere (determined by Bragg's law) and approach asymptotically the two spheres centered at the origin O and at the reciprocal node H , with a refraction-corrected radius, $k_0(1-\Gamma F_0/2)$. The two corresponding spheres in vacuum (outside crystal) are

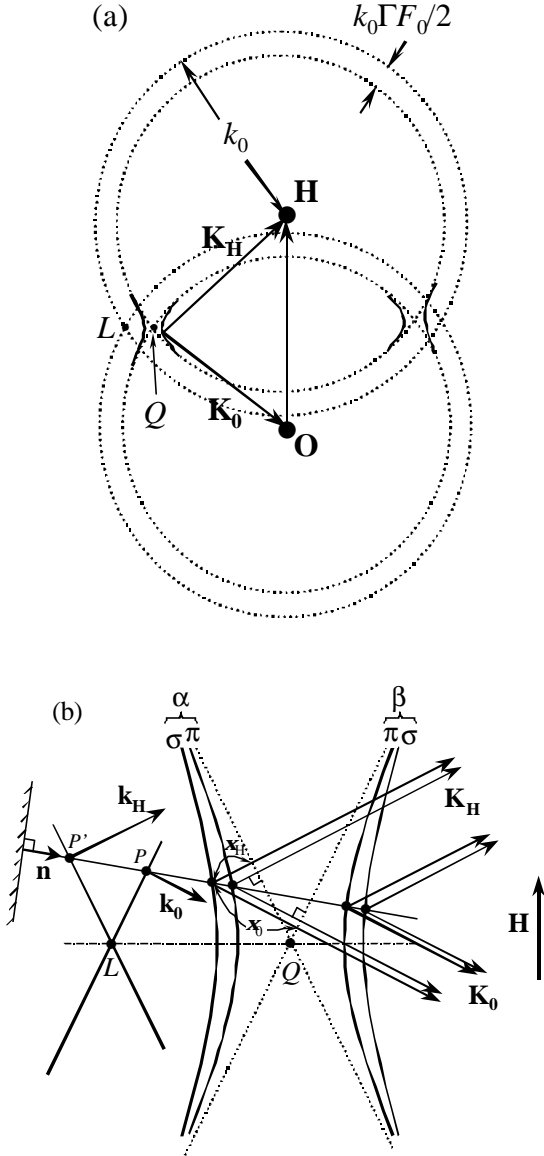


Figure 2: Dispersion surface in the two-beam case. (a) Overview. (b) Close-up view around the intersection region.

also shown and their intersection point is usually called the Laue point, L . The dispersion surface branches closer to the Laue point are called the α branches ($\alpha\sigma$, $\alpha\pi$), and those further from the Laue point are called the β branches ($\beta\sigma$, $\beta\pi$). Since the square root value of the right-hand side constant in Eq.(11) is much less than k_0 , the gap at the diameter point is on the order of 10^{-3} compared to the radius of the spheres. Therefore, the spheres can be viewed essentially as planes in the vicinity of the diameter point, as illustrated in Fig.2(b). However, the curvatures have to be considered when the Bragg reflection is in the glancing angle geometry (see Section V).

(2) **Wave field amplitude ratios:** In addition to the wavevectors, the eigenvalue equation (9) also provides the ratio of the wave field amplitudes inside the crystal for each polarization. In terms of \mathbf{x}_0 and \mathbf{x}_H , the amplitude ratio is given by

$$D_H/D_0 = -2\mathbf{x}_0/k_0\Gamma PF_{\bar{H}} = -k_0\Gamma PF_H/2\mathbf{x}_H. \quad (12)$$

Again the actual ratio in the crystal depends entirely on the tie points selected by the boundary conditions. Around the diameter point \mathbf{x}_0 and \mathbf{x}_H have similar lengths and thus the field amplitudes D_H and D_0 are comparable. Away from the exact Bragg condition, only one of \mathbf{x}_0 and \mathbf{x}_H has an appreciable size and thus either D_0 or D_H dominates according to their asymptotic spheres.

(3) **Boundary conditions and Snell's law:** To illustrate how tie points are selected by Snell's law in the two-beam case, we consider the situation in Fig.2(b) where a crystal surface is indicated by a shaded line. We start with an incident condition corresponding to an incident vacuum wavevector \mathbf{k}_0 at point P . We then construct a surface normal passing through P and intersecting four tie points on the dispersion surface. Because of the Snell's law, the wavefields associated with these four points are the only permitted waves inside the crystal. There are four waves for each reciprocal node, O or H , altogether a total of eight waves may exist inside the crystal in the two-beam case. To find the external diffracted beam, we follow the same surface normal to the intersection point P' , and the corresponding wavevector connecting P' to the reciprocal node H would be the diffracted beam that we can measure with a detector outside the crystal.

Depending on whether or not a surface normal intercepts both α and β branches at the same incident condition, a diffraction geometry is called either the Laue transmission or the Bragg reflection case. In terms of the direction cosines g_0 and g_H of the external incident and diffracted wavevectors, \mathbf{k}_0 and \mathbf{k}_H , with respect to the surface normal \mathbf{n} , it is useful to define a parameter b :

$$b \equiv g_0/g_H \equiv \mathbf{k}_0 \cdot \mathbf{n} / \mathbf{k}_H \cdot \mathbf{n},$$

where $b > 0$ corresponds to the Laue case and $b < 0$ the Bragg case. The cases with $b = \pm 1$ are called the symmetric Laue or Bragg cases, and for that reason b is often called the *asymmetry factor*.

(4) Poynting's vector and energy flow: The question about the energy flow directions in dynamical diffraction is of fundamental interests to scientists who use x-ray topography to study defects in perfect crystals. Energy flow of an electromagnetic wave is determined by its time-averaged Poynting vector, defined as

$$\mathbf{S} = \frac{c}{8\pi} (\mathbf{E} \times \mathbf{H}^*) = \frac{c}{8\pi} |\mathbf{D}|^2 \hat{\mathbf{K}},$$

where c is the speed of light, $\hat{\mathbf{k}}$ is a unit vector along the propagation direction, and terms on the order of Γ or higher are ignored. The total Poynting vector \mathbf{S}_T at each tie point on each branch of the dispersion surfaces is the vector sum of those for the **O**-beam and the **H**-beam:

$$\mathbf{S}_T = \frac{c}{8\pi} (D_0^2 \hat{\mathbf{K}}_0 + D_H^2 \hat{\mathbf{K}}_H).$$

To find the direction of \mathbf{S}_T , we consider the surface normal \mathbf{v} of the dispersion branch, which is along the direction of the gradient of dispersion equation Eq.(11):

$$\begin{aligned} \mathbf{v} &= \nabla(x_0 x_H) = x_0 \nabla x_H + x_H \nabla x_0 = \frac{x_0}{x_H} \hat{\mathbf{K}}_H + \frac{x_H}{x_0} \hat{\mathbf{K}}_0 \\ &\propto D_0^2 \hat{\mathbf{K}}_0 + D_H^2 \hat{\mathbf{K}}_H \propto \mathbf{S}_T, \end{aligned}$$

where we have used Eq.(12) and assumed a negligible absorption ($|F_{-H}| = |F_H|$). Thus we conclude that \mathbf{S}_T is parallel to \mathbf{v} , the normal to the dispersion surface. In another word, the total energy flow at a given tie point is always normal to the local dispersion surface. This important theorem is valid in general and was first proved by Kato (1960). It follows that the energy flow inside the crystal is parallel to the atomic planes at the full excitation condition, i.e. the diameter points of the hyperboloids.

Special Dynamical Effects

There are significant differences in the physical diffraction processes between the kinematic theory and the dynamical theory. The most striking observable results from the dynamical theory are Pendellösung fringes, anomalous transmission, finite reflection width for semi-infinite crystals, x-ray standing waves, and x-ray birefringence. With the aid of dispersion surface shown in Fig.2, these effects can be explained without formally solving the mathematical equations.

(1) Pendellösung: In a Laue case, the **a** and **b** tie points across the diameter gap of the hyperbolic dispersion surfaces are excited simultaneously at a given incident condition. The two sets of travelling waves associated with the two branches can interfere with each other and cause oscillations in the diffracted intensity as the thickness of the crystal changes on the order of $2\pi/\Delta K$, where ΔK is simply the gap at the diameter point. These intensity oscillations are termed *Pendellösung* fringes and the quantity $2\pi/\Delta K$ is called the *Pendellösung period*. From the geometry shown in Fig.2(b), it is straightforward to show that the diameter gap is given by

$$\Delta K = k_0 \Gamma |P| \sqrt{F_H F_{\bar{H}}} / \cos q_B,$$

where q_B is the internal Bragg angle. As an example, at 10 keV, for Si (111) reflection, $\Delta K = 2.67 \times 10^{-5} \text{ \AA}^{-1}$, and thus the Pendellösung period is $2\pi/\Delta K = 23 \mu\text{m}$.

Pendellösung interference is a unique diffraction phenomenon for the Laue geometry. Both the diffracted wave (**H**-beam) and the forward-diffracted wave (**O**-beam) are affected by this effect. The intensity oscillations for these two beams are 180° out of phase to each other, creating the effect of energy flow swapping back and forth between the two directions as a function of depth into the crystal surface. For more detailed discussions of *Pendellösung* fringes we refer to a review by Kato (1974).

We should point out that Pendellösung fringes are entirely different in origin from interference fringes due to crystal thickness. The thickness fringes are often observed in reflectivity measurements on thin film materials and can be mostly accounted for by finite size effect in Fraunhofer diffraction. The period of thickness fringes depends only on thickness, not on the strength of the reflection, while the Pendellösung period depends only on the reflection strength not on crystal thickness.

(2) Anomalous transmission: The four waves selected by tie points in the Laue case have different effective absorption coefficients. This can be understood qualitatively from the locations of the four dispersion surface branches relative to the vacuum Laue point L and to the average refraction-corrected point Q . The β branches are further from L and are on the more-refractive side of Q . Therefore the waves associated with the β branches have larger-than-average refraction and absorption. The α branches, on the other hand, are located closer to L and on the less-refractive side of Q , and therefore the waves on the α branches have less-than-average refraction and absorption. For a relatively thick crystal in the Laue diffraction geometry, effectively the α waves would be able to pass through the thickness of the crystal "easier" than an average wave would. What this implies is that if no intensity is observed in the transmitted beam at off-Bragg conditions, an

anomalously “transmitted” intense beam can actually appear when the crystal is set to a strong Bragg condition. This phenomenon is called the anomalous transmission and was first observed by Borrmann (1950) and often is also called the Borrmann effect.

If the Laue crystal is sufficiently thick, then even the $\alpha\pi$ wave may be absorbed and only the $\alpha\sigma$ wave would remain. In this case the Laue diffracting crystal can be used as linear polarizer since only the **s**-polarized x-rays would be transmitted through the crystal.

(3) **Darwin width:** In a Bragg reflection geometry, all the excited tie points lie on the same branch of the dispersion surface at a given incident angle. Furthermore, no tie points can be excited at the center of a Bragg reflection, where a gap exists at the diameter point of the dispersion surfaces. The gap indicates that no internal traveling waves exist at the exact Bragg condition and total external reflection is the only outlet of the incident energy if absorption is ignored. In fact, the size of the gap determines the range of incident angles at which the total reflection would occur and this angular width is usually called the *Darwin width* of a Bragg reflection in perfect crystals. In the case of symmetric Bragg geometry, it is easy to see from Fig.2 that the full Darwin width is

$$w = \frac{\Delta K}{k_0 \sin q_B} = \frac{2\Gamma|P|\sqrt{F_H F_{\bar{H}}}}{\sin 2q_B}. \quad (13)$$

Typical values for w are on the order of a few arc-seconds.

The existence of a finite reflection width w even for a semi-infinite crystal may seem to contradict the mathematical theory of Fourier transforms which would give rise to a zero reflection width if the crystal size is infinite. In fact this is not the case. A more careful examination of the situation shows that because of the extinction the incident beam would never be able to see the whole “infinite” crystal. Thus the finite Darwin width is a direct result of the extinction effect in dynamical theory and is needed to conserve the total energy in the physical system.

(4) **X-ray standing waves (XSW):** Another important effect in dynamical diffraction is the x-ray standing waves (Batterman, 1964). Inside a diffracting crystal, the total wave field intensity is the coherent sum of the **O**-beam and the **H**-beam and is given by (**s** polarization):

$$|\mathbf{D}|^2 = \left| \mathbf{D}_0 e^{-i\mathbf{K}_0 \cdot \mathbf{r}} + \mathbf{D}_H e^{-i\mathbf{K}_H \cdot \mathbf{r}} \right|^2 = |\mathbf{D}_0|^2 \left| 1 + \frac{D_H}{D_0} e^{-i\mathbf{H} \cdot \mathbf{r}} \right|^2. \quad (14)$$

Eq.(14) represents a standing wave field with a spatial period of $2\pi/|\mathbf{H}|$ which is simply the d-spacing of the

Bragg reflection. The field amplitude ratio D_H/D_0 has well-defined phases at α and β branches of the dispersion surface. According to Eq.(12) and Fig.2, we see that the phase of D_H/D_0 is $\pi + \mathbf{a}_H$ at the α branch since \mathbf{x}_H is positive and \mathbf{a}_H at the β branch since \mathbf{x}_H is negative, where \mathbf{a}_H is the phase of the structure factor F_H and can be set to zero by a proper choice of real space origin. Thus the α mode standing wave has its *nodes* on the atomic planes and the β mode standing wave has its *antinodes* on the atomic planes.

In Laue transmission geometry, both the α and the β modes are excited simultaneously in the crystal. However, the β mode standing wave is attenuated more strongly because its peak field coincide with the atomic planes. This is the physical origin of the Borrmann anomalous absorption effect.

The standing waves also exist in the Bragg geometry. Because of its more recent applications in materials studies, we will devote a later segment to discuss this in some more details.

(5) **X-ray birefringence:** Being able to produce and to analyze a generally polarized electromagnetic wave has long benefited scientists and researchers in the field of visible light optics and in studying optical properties of materials. In the x-ray regime, however, such abilities have been very limited because of the weak interaction of x-rays with matter, especially for production and analysis of circularly-polarized x-ray beams. The situation has changed significantly in recent years. The growing interests in studying magnetic and anisotropic electronic materials by x-ray scattering and spectroscopic techniques have initiated many new developments in both the production and the analyses of specially polarized x-rays. The routinely available high-brightness synchrotron radiation sources can now provide naturally collimated x-rays which can be easily manipulated by special x-ray optics to generate x-ray beams with its polarization tunable from linear to circular. Such optics are usually called *x-ray phase plates* or *phase retarders*.

The principles of most x-ray phase plates are based on the linear birefringence effect near a Bragg reflection in perfect or nearly perfect crystals due to dynamical diffraction (Hart, 1978; Belyakov & Dmitrienko, 1989). As illustrated in Fig.2, close to a Bragg reflection \mathbf{H} , the lengths of the wavevectors for the **s** and the **p** polarizations are slightly different. The difference can cause a phase shift Δ between the **s** and the **p** wave fields to accumulate through the crystal thickness t : $\Delta = (K_\sigma - K_\pi)t$. When the phase shift Δ reaches $\pm 90^\circ$, circularly polarized radiation is generated, and such a device is called a *quarter-wave* phase plate or retarder (Mills, 1988; Hirano *et al.* 1991; Giles *et al.* 1994). In addition to these transmission-type phase retarders, a reflection-type phase plate has also been proposed and studied (Brummer *et al.* 1984; Batterman, 1992; Shastri *et al.* 1995), which has the advantage of being thickness-

independent. However, it has been demonstrated that the Bragg-transmission-type phase retarders are more robust to incident beam divergences and thus are very practical x-ray circular polarizers. They have been used for measurements of magnetic dichroism in hard permanent magnets and other magnetic materials (Giles *et al.* 1994; Lang *et al.* 1995). Recent reviews on x-ray polarizers and phase plates can be found in articles by Hart (1991), Hirano, Ishikawa & Kikuta (1995), Shen (1996), and Malgrange (1996).

Solution of Dispersion Equation

So far we have focused our discussions to the physical effects that exist in dynamical diffraction from perfect crystals and have tried to avoid the mathematical details of the solutions to the dispersion equation, Eq.(7) or (8). As we have shown, considerable physical insight to the diffraction processes can be gained without going into mathematical details. To obtain the diffracted intensities in dynamical theory, however, the mathematical solutions are unavoidable. In this segment we will summarize these results. We will keep the formulae in a general complex form so that absorption effects are automatically taken into account.

The key to solving the dispersion equations Eq.(10) or (11) is to realize that the internal incident beam \mathbf{K}_0 can only defer from the vacuum incident beam \mathbf{k}_0 by a small component \mathbf{K}_{0n} along the surface normal direction of the

incident surface, which in turn is linearly related to \mathbf{x}_0 or \mathbf{x}_H . The final expression reduces to a quadratic equation for \mathbf{x}_0 or \mathbf{x}_H , and solving for \mathbf{x}_0 or \mathbf{x}_H alone results in the following (Batterman & Cole, 1964):

$$\mathbf{x}_0 = \frac{1}{2} k_0 |P| \Gamma \sqrt{|b| F_H F_{\bar{H}}} \left[\mathbf{h} \pm (\mathbf{h}^2 + b/|b|)^{1/2} \right], \quad (15)$$

where \mathbf{h} is the *reduced deviation parameter* normalized to the Darwin's width:

$$\mathbf{h} \equiv \frac{2b}{w\sqrt{|b|}} (\Delta\mathbf{q} - \Delta\mathbf{q}_0),$$

$\Delta\mathbf{q} = \mathbf{q} - \mathbf{q}_B$ is the angular deviation from the vacuum Bragg angle \mathbf{q}_B , and $\Delta\mathbf{q}_0$ is the refraction correction:

$$\Delta\mathbf{q}_0 \equiv \frac{\Gamma F_0 (1 - 1/b)}{2 \sin 2\mathbf{q}_B}.$$

The dual signs in Eq.(15) correspond to the α and β branches of the dispersion surface. In the Bragg case, $b < 0$ so the correction $\Delta\mathbf{q}_0$ is always positive, i.e. the \mathbf{q} value at the center of a reflection is always slightly larger than \mathbf{q}_B given by the kinematic theory. In the Laue case the sign of $\Delta\mathbf{q}_0$ depends on whether $b > 1$ or $b < 1$. In the case of absorbing crystals, both \mathbf{h} and $\Delta\mathbf{q}_0$ can be complex and the directional properties are represented by the real parts of these complex variables while their imaginary parts are related to the absorption given by F_0'' and w .

Substituting Eq.(15) into Eq.(12) yields the wave field amplitude ratio inside the crystal as a function of \mathbf{h} :

$$\frac{D_H}{D_0} = -\frac{|P|}{P} \sqrt{|b| F_H / F_{\bar{H}}} \left[\mathbf{h} \pm (\mathbf{h}^2 + b/|b|)^{1/2} \right]. \quad (16)$$

Diffracted Intensities

We now employ the boundary conditions to evaluate the diffracted intensities.

(1) Boundary conditions: In the Laue transmission case [Fig.3(a)], assuming a plane wave with an infinite cross section, the field boundary conditions are given by the following equations:

$$\text{Entrance surface: } \begin{cases} \mathbf{D}_0^i = \mathbf{D}_{0a} + \mathbf{D}_{0b} \\ 0 = \mathbf{D}_{Ha} + \mathbf{D}_{Hb} \end{cases}, \quad (17)$$

$$\text{Exit surface: } \begin{cases} \mathbf{D}_0^e = \mathbf{D}_{0a} e^{-i\mathbf{K}_{0a} \cdot \mathbf{r}} + \mathbf{D}_{0b} e^{-i\mathbf{K}_{0b} \cdot \mathbf{r}} \\ \mathbf{D}_H^e = \mathbf{D}_{Ha} e^{-i\mathbf{K}_{Ha} \cdot \mathbf{r}} + \mathbf{D}_{Hb} e^{-i\mathbf{K}_{Hb} \cdot \mathbf{r}} \end{cases}. \quad (18)$$

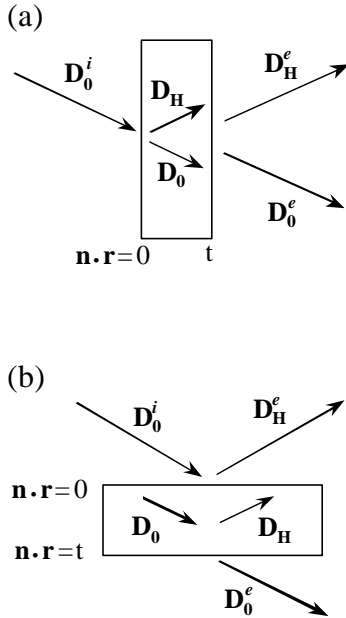


Figure 3: Boundary conditions for the wave fields outside the crystal in (a) Laue case and (b) Bragg case.

In the Bragg reflection case [Fig.3(b)], the field boundary condition is given by

$$\text{Entrance surface: } \begin{cases} \mathbf{D}_0^i = \mathbf{D}_{0a} + \mathbf{D}_{0b} \\ \mathbf{D}_H^e = \mathbf{D}_{Ha} + \mathbf{D}_{Hb} \end{cases}, \quad (19)$$

$$\text{Back surface: } \begin{cases} \mathbf{D}_0^e = \mathbf{D}_{0a} e^{-i\mathbf{K}_{0a} \cdot \mathbf{r}} + \mathbf{D}_{0b} e^{-i\mathbf{K}_{0b} \cdot \mathbf{r}} \\ 0 = \mathbf{D}_{Ha} e^{-i\mathbf{K}_{Ha} \cdot \mathbf{r}} + \mathbf{D}_{Hb} e^{-i\mathbf{K}_{Hb} \cdot \mathbf{r}} \end{cases}. \quad (20)$$

In either case, there are six unknowns, \mathbf{D}_{0a} , \mathbf{D}_{0b} , \mathbf{D}_{Ha} , \mathbf{D}_{Hb} , \mathbf{D}_0^e , \mathbf{D}_H^e , and three pairs of equations, (16), (17), (18), or (16), (19), (20), for each polarization state. Our goal is to express the diffracted waves \mathbf{D}_H^e outside the crystal as a function of the incident wave \mathbf{D}_0^i .

(2) *Intensities in the Laue case*: In the Laue transmission case, we obtain, apart from an insignificant phase factor, that

$$\mathbf{D}_H^e = \mathbf{D}_0^i e^{-\frac{m_t}{4} \left(\frac{1}{g_0} + \frac{1}{g_H} \right)} \sqrt{\frac{bF_H}{F_H}} \frac{\sin\left(A\sqrt{h^2+1}\right)}{\sqrt{h^2+1}},$$

where A is the effective thickness (complex) that relates to real thickness t by (Zachariasen, 1945)

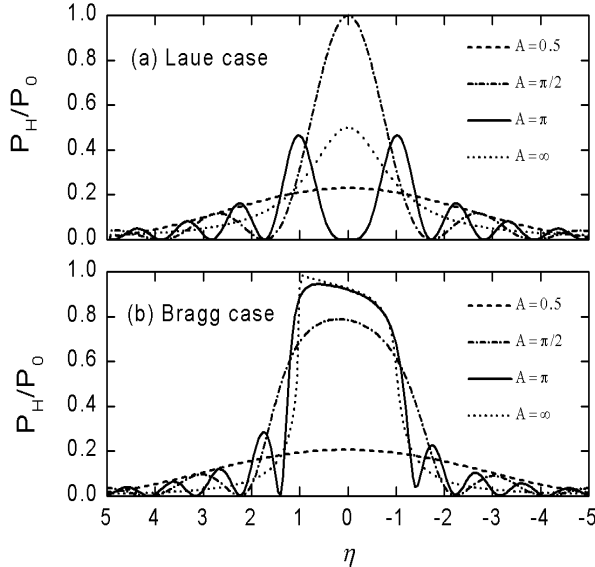


Figure 4: Diffracted intensity P_H/P_0 in (a) non-absorbing Laue case, and (b) absorbing Bragg case, for several effective thicknesses. The Bragg reflection in (b) is for GaAs (220) at $l = 1.48$ Å.

$$A \equiv \frac{p\Gamma|P|t\sqrt{F_H F_{\bar{H}}}}{l\sqrt{|g_0 g_H|}}.$$

The real part of A is essentially the ratio of the crystal thickness to the Pendellösung period.

A quantity often measured in experiments is the total power P_H in the diffracted beam, which equals to the diffracted intensity multiplied by the cross-section area of the beam. The power ratio P_H/P_0 of the diffracted beam to the incident beam is given by the intensity ratio, $|\mathbf{D}_H^e/\mathbf{D}_0^i|^2$, multiplied by the area ratio, $1/|b|$, of the beam cross-sections:

$$\frac{P_H}{P_0} = \frac{1}{|b|} \left| \frac{\mathbf{D}_H^e}{\mathbf{D}_0^i} \right|^2 = e^{-\frac{m_t}{2} \left(\frac{1}{g_0} + \frac{1}{g_H} \right)} \left| \frac{F_H}{F_{\bar{H}}} \right| \frac{\left| \sin\left(A\sqrt{h^2+1}\right) \right|^2}{|h^2+1|}. \quad (21)$$

A plot of P_H/P_0 versus h is usually called the rocking curve. Keeping in mind that h can be a complex variable due essentially to F_0'' , Eq.(21) is a general expression that is valid for both non-absorbing and absorbing crystals. A few examples of the rocking curves in the Laue case for non-absorbing crystals are shown in Fig.4(a).

For thick non-absorbing crystals, A is large ($A \gg 1$) so the \sin^2 oscillations tend to average to a value equal to $1/2$. Thus Eq.(21) reduces to a simple Lorentzian shape:

$$\frac{P_H}{P_0} = \frac{1}{2(h^2+1)}.$$

For thin non-absorbing crystals, $A \ll 1$, we rewrite Eq.(21) in the following form:

$$\frac{P_H}{P_0} = \left[\frac{\sin\left(A\sqrt{h^2+1}\right)}{\sqrt{h^2+1}} \right]^2 \approx \left[\frac{\sin(Ah)}{h} \right]^2.$$

The above approximation can be realized by expanding the quantities in the square brackets on both sides to third power and neglecting the A^3 term since $A \ll 1$. We see that in this thin crystal limit, the dynamical theory gives the same result as the kinematic theory. The condition $A \ll 1$ can be restated as the crystal thickness t is much less than the Pendellösung period.

(3) *Intensities in the Bragg case*: In the Bragg reflection case, we obtain that the diffracted wave field is given by:

$$\mathbf{D}_H^e = \mathbf{D}_0^i \sqrt{\frac{bF_H}{F_{\bar{H}}}} \frac{1}{h + i\sqrt{h^2-1} \cot\left(A\sqrt{h^2-1}\right)}.$$

The power ratio P_H/P_0 of the diffracted beam to the incident, often called the *Bragg reflectivity*, is

$$\frac{P_H}{P_0} = \left| \frac{F_H}{F_{\bar{H}}} \right| \frac{1}{\left| h + i\sqrt{h^2 - 1} \cot\left(A\sqrt{h^2 - 1}\right) \right|^2}. \quad (22)$$

In the case of thick crystals, $A \gg 1$, Eq.(19) reduces to

$$\frac{P_H}{P_0} = \left| \frac{F_H}{F_{\bar{H}}} \right| \frac{1}{\left| h \pm \sqrt{h^2 - 1} \right|^2}. \quad (23)$$

The choice of the signs is such that a smaller value of P_H/P_0 is retained.

On the other hand, for semi-infinite crystals ($A \gg 1$), we can go back to the boundary conditions Eqs.(19) and (20) and ignore the back surface all together. If we then apply the argument that only one of the two tie points on each branch of the dispersion surface is physically feasible in the Bragg case because of the energy flow conservation, we arrive at the following simple boundary condition:

$$\mathbf{D}_0^i = \mathbf{D}_0, \quad \mathbf{D}_H^e = \mathbf{D}_H.$$

Using the above equation and Eq.(16), the diffracted power can be expressed by

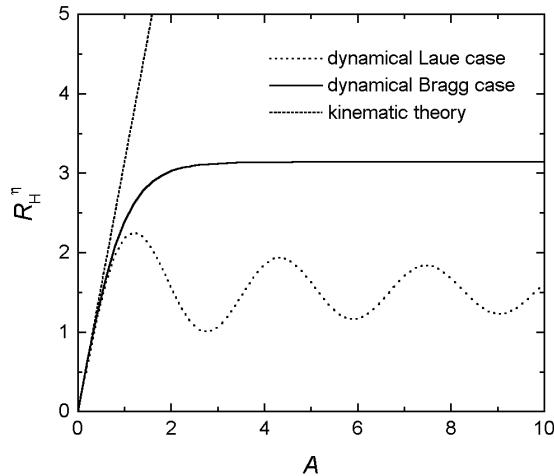


Figure 5: Comparison of integrated intensities in the Laue case and the Bragg case with the kinematic theory.

$$\frac{P_H}{P_0} = \left| \frac{F_H}{F_{\bar{H}}} \right| \left| h \pm \sqrt{h^2 - 1} \right|^2. \quad (24)$$

Again the sign in front of the square root is chosen so that P_H/P_0 is less than unity. The result is obviously identical to Eq.(23).

Far away from the Bragg condition, $h \gg 1$, Eq.(23) shows that the reflected power decreases as $1/h^2$. This asymptotic form represents the *tails* of a Bragg reflection (Andrews & Cowley, 1985) which are also called the *crystal truncation rod* in the kinematic theory (Robinson, 1986). In reciprocal space the direction of the tails is along the surface normal since the diffracted wavevector can only defer from the Bragg condition by a component normal to the surface or interface. More detailed discussions of the crystal truncation rods in dynamical theory can be found in Colella (1991), Caticha (1993, 1994) and Durbin (1995).

Examples of the reflectivity curves Eq.(22) for a GaAs crystal with different thicknesses in the symmetric Bragg case are shown in Fig.4(b). The oscillations in the tails are entirely due to the thickness of the crystal. These modulations are routinely observed in x-ray diffraction profiles from semiconductor thin films on substrates and can be used to determine the thin film thickness very accurately (Fewster, 1996).

(4) Integrated intensities: The integrated intensity R_H^η in the reduced h units is given by integrating the diffracted power ratio P_H/P_0 over the entire h range.

For non-absorbing crystals in the Laue case, in the limiting cases of $A \ll 1$ and $A \gg 1$, R_H^η can be calculated analytically as (Zachariasen, 1945)

$$R_H^h = \int_{-\infty}^{\infty} \left(\frac{P_H}{P_0} \right) dh = \begin{cases} pA, & A \ll 1 \\ p/2. & A \gg 1 \end{cases}$$

For intermediate values of A or for absorbing crystals, the integral can only be calculated numerically. A general plot of R_H^η versus A in the non-absorbing case is shown in Fig.5 as the dotted line.

For non-absorbing crystals in the Bragg case, Eq.(22) can be integrated analytically (Darwin, 1922) to yield

$$R_H^h = \int_{-\infty}^{\infty} \left(\frac{P_H}{P_0} \right) dh = p \tanh(A) = \begin{cases} pA, & A \ll 1 \\ p. & A \gg 1 \end{cases}$$

A plot of the integrated power in the symmetric Bragg case is shown in Fig.5 as the solid curve. Both curves in Fig.5 show a linear behavior for small A , which is consistent with the kinematic theory.

Using the definitions of h and A , we obtain that the integrated power R_H^θ over the incident angle \mathbf{q} in the limit of $A \ll 1$ is given by

$$R_H^q = \int_{-\infty}^{\infty} \left(\frac{P_H}{P_0} \right) d\mathbf{q} = \frac{w}{2} R_H^h = \frac{\mathbf{p}}{2} wA = \frac{r_e^2 I^3 P^2 |F_H|^2 t}{V_c \sin 2\mathbf{q}_B},$$

which is identical to the integrated intensity in the kinematic theory for a small crystal (Warren, 1969). Thus in some sense the kinematic theory is a limiting form of the dynamical theory, and the departures of the integrated intensities at larger A values (Fig.5) is simply the effect of primary extinction. In the thick crystal limit $A \gg 1$, the \mathbf{q} -integrated intensity R_H^0 in both Laue and Bragg cases is linear in $|F_H|$. This linear rather than quadratic dependence on $|F_H|$ is a distinct and characteristic result of dynamical diffraction.

Standing Waves

As we discussed earlier, near or at a Bragg reflection, the wave field amplitudes, Eq.(14), represent standing

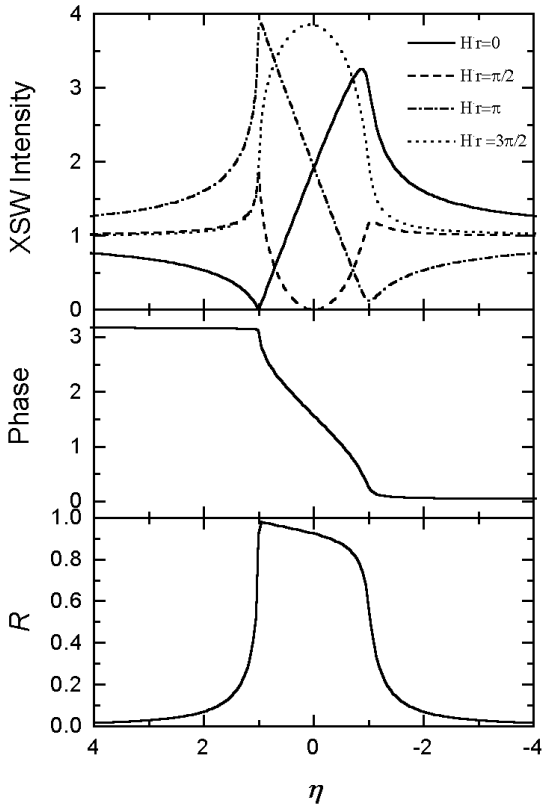


Figure 6: XSW intensity and phase as a function of reduced angular parameter \mathbf{h} , along with reflectivity curve, calculated for a semi-infinite GaAs (220) reflection at 1.48 Å.

waves inside the diffracting crystal. In the Bragg reflection geometry, as the incident angle increases through the full Bragg reflection, the selected tie points shift from α branch to β branch. Therefore the nodes of the standing wave shift from on the atomic planes ($r=0$) to in-between the atomic planes ($r=d/2$) and the corresponding antinodes shift from in-between to on the atomic planes.

For a semi-infinite crystal in the symmetric Bragg case and \mathbf{s} -polarization, the standing wave intensity can be written as, using Eqs.(14), (16) and (24):

$$I = \left| 1 + \sqrt{\frac{P_H}{P_0}} e^{i(n + \mathbf{a}_H - \mathbf{H} \cdot \mathbf{r})} \right|^2, \quad (25)$$

where n is the the phase of $\mathbf{h} \pm \sqrt{\mathbf{h}^2 - 1}$ and \mathbf{a}_H is the phase of the structure factor F_H , assuming absorption is negligible. If we define the diffraction plane by choosing an origin such that \mathbf{a}_H is zero, then the standing wave intensity as a function of \mathbf{h} is determined by the phase factor $\mathbf{H} \cdot \mathbf{r}$ with respect to the origin chosen and the d -spacing of the Bragg reflection (Bedzyk & Materlik, 1985). Typical standing wave intensity profiles given by Eq.(25) are shown in Fig.6. Also shown in Fig.6 are the phase variable n and the corresponding reflectivity curve.

A x-ray standing wave profile can be observed by measuring the x-ray fluorescence profile from atoms embedded in the crystal structure since the fluorescence signal is directly proportional to the internal wave field intensity at the atom position (Batterman, 1964). By analyzing the shape of a fluorescence profile the position of the fluorescing atom with respect to the diffraction plane can be determined. A detailed discussion of nodal plane position shifts of the standing waves in general absorbing crystals has been given by Authier (1986).

The standing wave technique has been used to determine foreign atom positions in bulk materials (Batterman, 1969; Golovchenko *et al.* 1974; Lagomarsino *et al.*, 1984; Kovalchuk & Kohn, 1986). Most recent applications of the XSW technique have been the determination of foreign atom positions, surface relaxations and disorders at crystal surfaces and interfaces (Durbin *et al.* 1986; Zegenhagen *et al.* 1988; Bedzyk *et al.* 1989; Martines *et al.* 1992; Fontes *et al.* 1993; Franklin *et al.* 1995; Lyman & Bedzyk, 1997). By measuring standing wave patterns for two or more reflections (either separately or simultaneously) along different crystallographic axes, atomic positions can be triangulized in space (Berman *et al.* 1987; Greiser & Materlik, 1986). More details of the XSW technique can be found in recent reviews given by Patel (1996) and Lagomarsino (1996).

The formation of x-ray standing waves is not restricted to wide-angle Bragg reflections in perfect

crystals. Bedzyk *et al.* (1988) has extended the technique to the regime of specular reflections from mirror surfaces, in which case both the phase and the period of the standing waves vary with the incident angle. Standing waves have also been used to study the spatial distribution of atomic species in mosaic crystals (Durbin, 1988) and in quasicrystals (Chung & Durbin, 1995; Jack *et al.*, 1997). Due to a substantial (although imperfect) standing wave formation, anomalous transmission has been observed on the strongest diffraction peaks in nearly perfect quasicrystals (Kycia *et al.*, 1993).

IV. MULTIPLE-BEAM DIFFRACTION

So far we have restricted our discussion to diffraction cases in which only the incident beam and one Bragg diffracted beam are present. There are experimental situations, however, in which more than one diffracted beams may be significant and therefore the two-beam approximation is no longer valid. These situations involve *multiple-beam diffraction* and are dealt with in this Section.

Basic Concepts

Multiple-beam diffraction occurs when several sets of atomic planes satisfy the Bragg's laws simultaneously. A convenient way to realize this is to excite one Bragg reflection \mathbf{H} and then rotate the crystal around the

diffraction vector \mathbf{H} . While the \mathbf{H} reflection is always excited during such a rotation, it is possible to bring another set of atomic planes, \mathbf{L} , into its diffraction condition and thus to have multiple-beam diffraction process. The rotation around the scattering vector \mathbf{H} is defined by an azimuthal angle, γ . For x-rays, multiple-beam diffraction peaks excited in this geometry was first observed by Renninger (1937) and often these multiple reflection peaks are also called the *Renninger peaks*. For electrons, multiple-beam diffraction situations exist in almost all cases because of the much stronger interactions between electrons and atoms.

As shown in Fig.7, if atomic planes \mathbf{H} and \mathbf{L} are both excited at the same time, then there is always another set of planes, $\mathbf{H-L}$, also in diffraction condition. The diffracted beam \mathbf{k}_L by \mathbf{L} reflection can be scattered again by the $\mathbf{H-L}$ reflection and this *doubly* diffracted beam is in the same direction as the \mathbf{H} -reflected beam \mathbf{k}_H . In this sense, the photons (or particles) in the doubly diffracted beam have been through a “detour” route compared to the *singly* diffracted photons (particles) by the \mathbf{H} reflection. We usually call \mathbf{H} the main reflection, \mathbf{L} the detour reflection, and $\mathbf{H-L}$ the coupling reflection.

Depending on the strengths of the structure factors involved, a multiple reflection can cause either an intensity enhancement (peak) or reduction (dip) in the two beam intensity of \mathbf{H} . A multiple reflection peak is commonly called the *Umweganregung* (‘detour’ in German) and a dip is called the *Aufhellung*. The former occurs when \mathbf{H} is relatively weak and both \mathbf{L} and $\mathbf{H-L}$ are strong, while the latter occurs when both \mathbf{H} and \mathbf{L} are strong and $\mathbf{H-L}$ is weak. A semi-quantitative intensity calculation can be obtained by total energy balancing among the multiple beams, as worked out by Moon & Shull (1964) and Zachariasen (1965).

In most experiments, multiple reflections are simply the nuisance that one tries to avoid since they cause inaccurate intensity measurements. In the last two decades, however, there have been renewed and increasing interests in multiple-beam diffraction because of its promising potential as a physical solution to the well-known *phase problem* in diffraction and crystallography. The phase problem refers to the fact that the data collected in a conventional diffraction experiment are the *intensities* of the Bragg reflections from a crystal, which are related only to the magnitude of the structure factors, and the *phase* information is lost. This is a classic problem in diffraction physics and its solution remains to be the most difficult part of a structure determination of materials, especially for biological macromolecular crystals. Due to an interference effect among the simultaneously excited Bragg beams, multiple-beam diffraction contains the direct phase information on the structure factors involved and therefore can be used as a way to solve the phase problem.

The basic idea of using multiple-beam diffraction to solve the phase problem was first proposed by Lipcomb

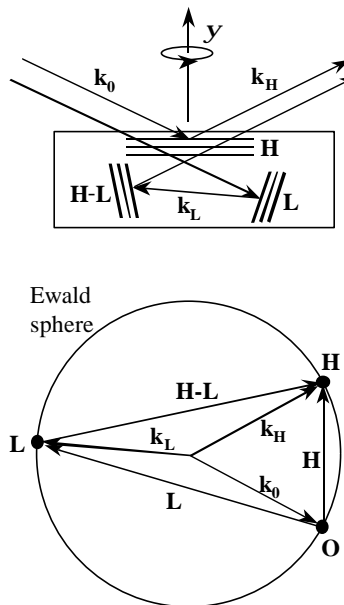


Figure 7: Illustration of a 3-beam diffraction case involving \mathbf{O} , \mathbf{H} , and \mathbf{L} , in real space (upper) and reciprocal space (lower).

(1949), and was first demonstrated by Colella (1974) in theory and by Post (1977) in an experiment on perfect crystals. The method was then further developed by several groups (Chapman, Yoder & Colella, 1981; Chang, 1982; Schmidt & Colella, 1985; Shen & Colella, 1987; 1988; Hummer, Weckert & Bondza, 1990) to show that the technique can be applied not only to perfect crystals but also to real, mosaic crystals. Recently, there have been considerable efforts to apply the multi-beam diffraction to large unit-cell inorganic and macromolecular crystals (Lee & Colella, 1993; Chang *et al.*, 1991; Hummer, Schwegle & Wechert, 1991; Wechert, Schwegle & Hummer, 1993). Progress in this area has been amply reviewed by Chang (1984, 1992), Colella (1995, 1996), and Weckert & Hummer (1997). A recent experimental innovation in reference-beam diffraction (Shen, 1998) allows parallel data-collection of three-beam interference profiles using an area detector in a modified oscillation-camera setup, and makes it possible to measure the phases of a large number of Bragg reflections in a relatively short time period.

Theoretical treatment of multiple-beam diffraction is considerably more complicated than the two-beam theory, as evidenced by some of the early works (Ewald & Heno, 1968). This is particularly so in the case of x-rays because of mixing of \mathbf{s} and \mathbf{p} polarization states in a multiple-beam diffraction process. In 1974, based upon his earlier work for electron diffraction (1972), Colella developed a full dynamical theory procedure for multiple-beam diffraction of x-rays (1974) and a corresponding computer program called NBEAM. With Colella's theory, multiple-beam dynamical calculations have become more practical and more easily performed. On today's powerful computers and software and for not too many beams, the NBEAM program can be run in an almost trivial fashion, even on personal computers. We will outline the principles of the NBEAM procedure in the next segment.

NBEAM Theory

The fundamental equations for multiple-beam x-ray diffraction are the same as those in the two-beam theory, before the two-beam approximation is made. We can go back to Eq.(3), expand the double cross product, and rewrite it in the following form:

$$\left[\frac{k_0^2}{K_i^2} - (1 + \Gamma F_0) \right] \mathbf{D}_i + \Gamma \sum_{j \neq i} F_{i-j} [\mathbf{u}_i (\mathbf{u}_i \cdot \mathbf{D}_j) - \mathbf{D}_j] = 0, \quad (26)$$

(1) *Eigenequation for D-field components*: In order to properly express the components of all wavefield amplitudes, we define a polarization unit-vector coordinate system for each wave j :

$$\begin{aligned} \mathbf{u}_j &= \mathbf{K}_j / |\mathbf{K}_j| \\ \mathbf{s}_j &= \mathbf{u}_j \times \mathbf{n} / |\mathbf{u}_j \times \mathbf{n}|, \\ \mathbf{p}_j &= \mathbf{u}_j \times \mathbf{s}_j \end{aligned}$$

where \mathbf{n} is the surface normal. Multiplying Eq.(26) by \mathbf{s}_j and \mathbf{p}_j yields

$$\begin{aligned} \left[\frac{k_0^2}{K_i^2} - (1 + \Gamma F_0) \right] D_{i\mathbf{s}} &= \Gamma \sum_{j \neq i} F_{i-j} [(\mathbf{s}_j \cdot \mathbf{s}_i) D_{j\mathbf{s}} + (\mathbf{p}_j \cdot \mathbf{s}_i) D_{j\mathbf{p}}] \\ \left[\frac{k_0^2}{K_i^2} - (1 + \Gamma F_0) \right] D_{i\mathbf{p}} &= \Gamma \sum_{j \neq i} F_{i-j} [(\mathbf{s}_j \cdot \mathbf{p}_i) D_{j\mathbf{s}} + (\mathbf{p}_j \cdot \mathbf{p}_i) D_{j\mathbf{p}}] \end{aligned} \quad (27)$$

(2) *Matrix form of the eigenequation*: For an N -beam diffraction case, the above equation can be written in a matrix form if we define a $2N \times 1$ vector $\underline{\mathbf{D}} = (D_{1\sigma}, \dots, D_{N\sigma}, D_{1\pi}, \dots, D_{N\pi})$, a $2N \times 2N$ diagonal matrix $\underline{\mathbf{T}}_j$ with $T_{ii} = k_0^2 / K_i^2$ ($i=j$) and $T_{ij} = 0$ ($i \neq j$), and a $2N \times 2N$ general matrix $\underline{\mathbf{A}}_{ij}$ that takes all the other coefficients in front of the wave field amplitudes. Matrix $\underline{\mathbf{A}}$ is Hermitian if absorption is ignored, or symmetric if the crystal is centrosymmetric. Eq.(28) then becomes

$$(\underline{\mathbf{T}} + \underline{\mathbf{A}}) \underline{\mathbf{D}} = 0.$$

This equation is equivalent to

$$(\underline{\mathbf{T}}^{-1} + \underline{\mathbf{A}}^{-1}) \underline{\mathbf{D}} = 0. \quad (29)$$

Strictly speaking the eigenvectors in Eq.(29) are actually the E-fields: $\underline{\mathbf{E}} = \underline{\mathbf{T}} \underline{\mathbf{D}}$. However $\underline{\mathbf{D}}$ and $\underline{\mathbf{E}}$ are exchangeable as discussed in Section II.

To find non-trivial solutions of Eq.(29), we need to solve the secular eigenvalue equation

$$|\underline{\mathbf{T}}^{-1} + \underline{\mathbf{A}}^{-1}| = 0, \quad (30)$$

with $T_{ii}^{-1} = K_i^2 / k_0^2$ ($i=j$) and $T_{ij}^{-1} = 0$ ($i \neq j$). We can write K_j^2 in the form of its normal (n) and tangential (t) components to the entrance surface:

$$K_j^2 = (K_{0n} + H_{jn})^2 + k_{jt}^2,$$

which is essentially the Bragg's law together with the boundary condition that $K_{jt} = k_{jt}$.

(3) *Strategy for numerical solutions*: Treating $m \equiv K_{0n} / k_0$ as the only unknown, Eq.(30) takes the following matrix form:

$$|m^2 - m\underline{\mathbf{B}} + \underline{\mathbf{C}}| = 0, \quad (31)$$

where $B_{ij} = -(2H_{jn}/k_0)\delta_{ij}$ is a diagonal matrix and $C_{ij} = (A^{-1})_{ij} + \delta_{ij}(H_{jn}^2 + k_{jt}^2)/k_0^2$. Eq.(31) is a quadratic eigenequation to which no computer routines are readily available for solving it. Colella in 1974 employed an ingenious method to show that Eq.(29) is equivalent to solving the following linear eigenvalue problem:

$$\begin{pmatrix} \mathbf{C} & \mathbf{0} \\ \mathbf{0} & \mathbf{D} \end{pmatrix} \begin{pmatrix} \mathbf{D}' \mathbf{e} \\ \mathbf{e} \end{pmatrix} = m \begin{pmatrix} \mathbf{D}' \mathbf{e} \\ \mathbf{e} \end{pmatrix}, \quad (32)$$

where \mathbf{I} is a unit matrix, and $\mathbf{D}' = m\mathbf{D}$ which is a redundant $2N$ vector with no physical significance.

Eq.(32) can now be solved with standard software routines that deal with linear eigenvalue equations. It is a $4N^{\text{th}}$ order equation for K_{0n} and thus has $4N$ solutions, denoted as K_{0n}^l , $l=1, \dots, 4N$. For each eigenvalue K_{0n} , there is a corresponding $2N$ -eigenvector that is stored in \mathbf{D} , which now is a $2N \times 4N$ matrix and its element labeled $D_{j\sigma}^l$ in its top N rows and $D_{j\pi}^l$ in its bottom N rows. These wave field amplitudes are evaluated at this point only on a relative scale, similar to the amplitude ratio in the two-beam case. For convenience, each $2N$ -eigenvector can be normalized to unity:

$$\sum_j^N \left(|D_{j\sigma}^l|^2 + |D_{j\pi}^l|^2 \right) = 1.$$

In terms of the eigenvalues K_{0n}^l and the eigenvectors $\mathbf{D}_j^l = (D_{j\sigma}^l, D_{j\pi}^l)$, a general expression for the wave field inside the crystal is given by

$$\mathbf{D}(\mathbf{r}) = \sum_l \mathbf{a}_l q_l \mathbf{a}_l \mathbf{D}_j^l e^{-i\mathbf{K}_j^l \cdot \mathbf{r}},$$

where $\mathbf{K}_j^l = \mathbf{K}_0^l + \mathbf{H}_j$ and q_l 's ($l=1, \dots, 4N$) are the coefficients to be determined by the boundary conditions.

(4) **Boundary conditions:** In general, it is not suitable to distinguish the Bragg and the Laue geometries in multiple-beam diffraction situations since it is possible to have an internal wavevector parallel to the surface and thus the distinction would be meaningless. The best way to treat the situation, as pointed out by Colella (1974), is to include both the back-diffracted and the forward-diffracted beams in vacuum, associated with each internal beam j . Thus for each beam j , we have two vacuum waves defined by $\mathbf{k}_{\pm j} = \mathbf{k}_{jt} \pm \mathbf{n}(k_0^2 - k_{jt}^2)^{1/2}$, where again the subscript t stands for the tangential component. Therefore for an N -beam diffraction from a parallel crystal slab, we have altogether $8N$ unknowns: $4N$ q_l 's for the field inside the crystal, $2N$ wave field components of \mathbf{D}_{-j}^e above the entrance surface, and $2N$ components of the wave field \mathbf{D}_j^e below the back surface.

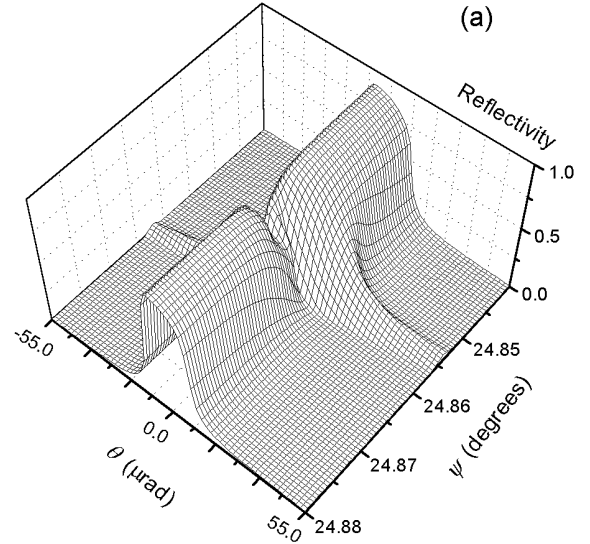
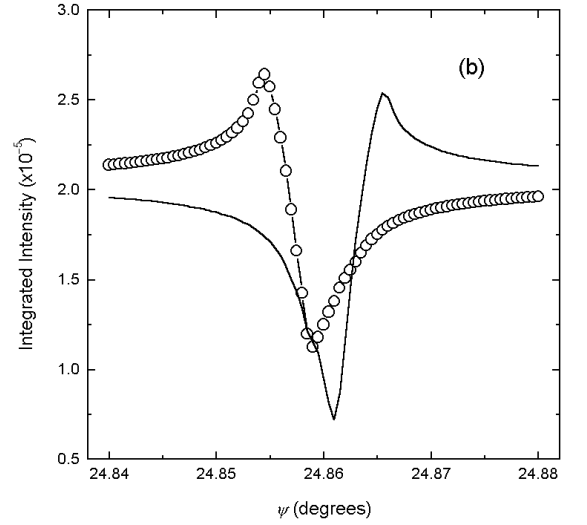


Figure 8: (a) Calculated reflectivity using NBEAM for the three-beam case of GaAs (335)/(551), as a function of Bragg angle \mathbf{q} and azimuthal angle \mathbf{y} . (b) Corresponding integrated intensities versus \mathbf{y} (open circles). The solid-line-only curve corresponds to the profile with an artificial phase of π added in the calculation.

The $8N$ equations needed to solve the above problem are fully provided by the general boundary conditions Eqs.(7). Inside the crystal we have $\mathbf{E}_j = \hat{\mathbf{a}}_l q_l \mathbf{D}_j^l e^{-i\mathbf{k}_j^l \cdot \mathbf{r}}$

and $\mathbf{H}_j = \mathbf{u}_j \times \mathbf{E}_j$, where the sum is over all eigenvalues l for each j -th beam. (We note that in Colella's original formalism converting \mathbf{D}_j to \mathbf{E}_j is not necessary since Eq.(29) is already for \mathbf{E}_j . This is also consistent with the omissions of all longitudinal components of \mathbf{E} -fields, *after eigenvalue equation is obtained*, in dynamical theory.) Outside the crystal, we have \mathbf{D}_j^e at the back surface and \mathbf{D}_j^e plus incident beam \mathbf{D}_0^i at the entrance surface. These boundary conditions provide 8 scalar equations for each beam j , and thus the $8N$ unknowns can be solved for as a function of \mathbf{D}_0^i .

(5) **Intensity computations:** Both the reflected and the transmitted intensities, I_r and I_t , for each beam j can be calculated by taking $I_j = |\mathbf{D}_j^e|^2 / |\mathbf{D}_0^i|^2$. We should note that the whole computational procedure described above only evaluate the diffracted intensity at *one* crystal orientation setting with respect to the incident beam. To obtain meaningful information, the computation is usually repeated for a series of angular settings of the incident angle \mathbf{q} and the azimuthal angle \mathbf{y} . An example of such two-dimensional calculations is shown in Fig.8(a), which is for a 3-beam case, GaAs (335)/(551). In many experimental situations, the intensities in the \mathbf{q} direction is usually integrated either purposely or because of the divergence in the incident beam. In that case the integrated intensities versus the azimuthal angle \mathbf{y} is plotted, as shown in Fig.8(b).

Second-Order Born Approximation

From the last segment, we see that the integrated intensity as a function of azimuthal angle usually displays an asymmetric intensity profile, due to the multiple-beam interference. The asymmetry profile contains the phase information about the structure factors involved. Although the NBEAM program provides full account for these multiple-beam interferences, it is rather difficult to see the physical insight of the process and the structural parameters it depends on.

In the past decade or so, there have been several approximate approaches for multiple-beam diffraction intensity calculations, based on Bethe approximations (Bethe, 1928; Juretschke, 1982; 1984; 1986; Hoier & Marthinsen, 1983), second-order Born approximation (Shen, 1986), Takagi-Taupin differential equations (Thorkildsen, 1987), and an expanded distorted-wave approximation (Shen, 1999b, 2000). In most of these approaches a modified two-beam structure factor can be defined so that integrated intensities can be obtained through the two-beam equations. In the following we will discuss only the second-order Born approximation (for x-rays) since it provides the most direct connection

to the two-beam kinematical results. The expanded distorted-wave theory is outlined at the end of this Unit following the standard distorted-wave theory in surface scattering.

To obtain the Born approximation series, we transform the fundamental equation (2) into an integral equation by using the Green's function and obtain the following:

$$\mathbf{D}(\mathbf{r}) = \mathbf{D}^{(0)}(\mathbf{r}) + \frac{1}{4\pi} \int d\mathbf{r}' \frac{e^{-ik_0|\mathbf{r}-\mathbf{r}'|}}{|\mathbf{r}-\mathbf{r}'|} \nabla' \times \nabla' \times [\mathbf{de}(\mathbf{r}')\mathbf{D}(\mathbf{r}')], \quad (33)$$

where $\mathbf{D}^{(0)}(\mathbf{r}) = \mathbf{D}_0^i e^{-i\mathbf{k}_0 \cdot \mathbf{r}}$ is the incident beam. Since \mathbf{de} is small, we can calculate the scattered wave field $\mathbf{D}(\mathbf{r})$ iteratively using the perturbation theory of scattering (Jackson, 1975). For first-order approximation, we substitute $\mathbf{D}(\mathbf{r}')$ in the integrand by the incident beam $\mathbf{D}^{(0)}(\mathbf{r}')$, and obtain a first-order solution $\mathbf{D}^{(1)}(\mathbf{r})$. This solution can then be substituted into the integrand again to provide a second-order approximation, $\mathbf{D}^{(2)}(\mathbf{r})$, and so on. The sum of all these approximate solutions gives rise to the true solution of Eq.(33):

$$\mathbf{D}(\mathbf{r}) = \mathbf{D}^{(0)}(\mathbf{r}) + \mathbf{D}^{(1)}(\mathbf{r}) + \mathbf{D}^{(2)}(\mathbf{r}) + \dots \quad (34)$$

This is essentially the Born series in quantum mechanics.

Assuming that the distance r from the observation point to the crystal is large compared to the size of the crystal (far field approximation), it can be shown (Shen, 1986) that the wave field of the first-order approximation is given by

$$\mathbf{D}^{(1)}(\mathbf{r}) = Nr_e F_{\mathbf{H}} \mathbf{u} \times (\mathbf{u} \times \mathbf{D}_0) \frac{e^{-ik_0 r}}{r}, \quad (35)$$

where N is the number of unit cells in the crystal, and only one set of atomic planes \mathbf{H} satisfies the Bragg's condition, $k_0 \mathbf{u} = \mathbf{k}_0 + \mathbf{H}$, with \mathbf{u} being a unit vector. Eq.(35) is identical to the scattered wave field expression in the kinematic theory, which is what we expect from the first order Born approximation.

To evaluate the second-order expression, we cannot use Eq.(35) as $\mathbf{D}^{(1)}$ since it is valid only in the far field. The original form of $\mathbf{D}^{(1)}$ with the Green's function has to be used. For detailed derivations we refer to Shen's article (1986). The final second-order wave field $\mathbf{D}^{(2)}$ is expressed by

$$\mathbf{D}^{(2)} = -Nr_e \frac{e^{-ik_0 r}}{r} \mathbf{u} \times \left[\mathbf{u} \times \Gamma \sum_{\mathbf{L}} F_{\mathbf{H}-\mathbf{L}} F_{\mathbf{L}} \frac{\mathbf{k}_{\mathbf{L}} \times (\mathbf{k}_{\mathbf{L}} \times \mathbf{D}_0)}{k_0^2 - k_{\mathbf{L}}^2} \right]. \quad (36)$$

It can be seen that $\mathbf{D}^{(2)}$ is the detoured wave field involving \mathbf{L} and $\mathbf{H-L}$ reflections, and the summation over \mathbf{L} represents a coherent superposition of all possible 3-beam interactions. The relative strength of a given detoured wave is determined by its structure factors and is inversely proportional to the distance $k_0^2 - k_L^2$ of the reciprocal lattice node \mathbf{L} from the Ewald sphere.

The total diffracted intensity up to second order in Γ is given by a coherent sum of $\mathbf{D}^{(1)}$ and $\mathbf{D}^{(2)}$:

$$I = \left| \mathbf{D}^{(1)} + \mathbf{D}^{(2)} \right|^2 = \left| Nr_e \frac{e^{-ik_0 r}}{r} \mathbf{u} \times \left[\mathbf{u} \times F_H \left(\mathbf{D}_0 - \Gamma \sum_{\mathbf{L}} \frac{F_{H-L} F_L}{F_H} \frac{\mathbf{k}_L \times (\mathbf{k}_L \times \mathbf{D}_0)}{k_0^2 - k_L^2} \right) \right] \right|^2. \quad (37)$$

Eq.(37) provides an approximate analytical expression for multiple-beam diffracted intensities and represents a modified two-beam intensity influenced by multiple-beam interactions. The integrated intensity can be computed by replacing F_H in the kinematic intensity formula by a ‘modified structure factor’ defined by

$$F_H \mathbf{D}_0 \rightarrow F_H \left(\mathbf{D}_0 - \Gamma \sum_{\mathbf{L}} \frac{F_{H-L} F_L}{F_H} \frac{\mathbf{k}_L \times (\mathbf{k}_L \times \mathbf{D}_0)}{k_0^2 - k_L^2} \right).$$

Often in practice, multiple-beam diffraction intensities are normalized to the corresponding two-beam values. In this case Eq.(37) can be used directly since the prefactors in front of the square brackets will be canceled out. It can be shown (Shen, 1986) that Eq.(37) gives essentially the same result as the NBEAM, as long as the full 3-beam excitation points are excluded, indicating that the second-order Born approximation is indeed a valid approach to multiple-beam diffraction simulations. Eq.(37) becomes divergent at the exact three-beam excitation point $k_0 = k_L$. However, the singularity can be avoided numerically if we take into account absorption by introducing an imaginary part in the wavevectors.

Special Multi-Beam Effects

The second-order Born approximation not only provides an efficient computational technique, but also allows one to gain substantial insight to the physics involved in a multiple-beam diffraction process.

(1) **3-beam interactions as the leading dynamical effect:** The successive terms in the Born series Eq.(34) represent different levels of multiple-beam interactions. For example, $\mathbf{D}^{(0)}$ is simply the incident beam (\mathbf{O}), $\mathbf{D}^{(1)}$ consists of two-beam (\mathbf{O} , \mathbf{H}) diffraction, $\mathbf{D}^{(2)}$ involves three-beam (\mathbf{O} , \mathbf{H} , \mathbf{L}) interactions, and so on. Eq.(36) shows that even when more than three beams are involved, the *individual* three-beam interactions are the

dominant effects than higher-order-beam interactions. This conclusion is very important to computations of N beam effects when N is large. It can greatly simplify even the full dynamical calculations using NBEAM, as shown by Tischler & Batterman (1986). The new multiple-beam interpretation of the Born series also implies that the three-beam effect is the leading term beyond the kinematic first-order Born approximation and thus is the dominant dynamical effect in diffraction. In a sense, the three-beam interactions ($\mathbf{O} \Rightarrow \mathbf{L} \Rightarrow \mathbf{H}$) are even more important than the multiple scattering in the two-beam case since it involves $\mathbf{O} \Rightarrow \mathbf{H} \Rightarrow \mathbf{O} \Rightarrow \mathbf{H}$ (or higher-order) scattering which is equivalent to a four-beam interaction.

(2) **Phase information:** Eq.(37) shows explicitly the phase information involved in the multiple-beam diffraction. The interference between the detoured wave $\mathbf{D}^{(2)}$ and the directly scattered wave $\mathbf{D}^{(1)}$ depends on the relative phase difference between the two waves. This phase difference is equal to phase \mathbf{n} of the denominator, plus the phase triplet \mathbf{d} of the structure factor phases \mathbf{a}_{H-L} , \mathbf{a}_L and \mathbf{a}_H :

$$\mathbf{d} = \mathbf{a}_{H-L} + \mathbf{a}_L - \mathbf{a}_H.$$

It can be shown that although the individual phases \mathbf{a}_{H-L} , \mathbf{a}_L and \mathbf{a}_H , depend on the choice of origin in the unit cell, the phase triplet \mathbf{d} does not and is therefore called the *invariant phase triplet* in crystallography. The resonant phase \mathbf{n} depends on whether the reciprocal node \mathbf{L} is outside ($k_0 < k_L$) or inside ($k_0 > k_L$) the Ewald sphere. As the diffracting crystal is rotated through a three-beam excitation, \mathbf{n} changes by π since \mathbf{L} is swept through the Ewald sphere. This phase change of π in addition to the constant phase triplet \mathbf{d} is the cause for the asymmetric 3-beam diffraction profiles and allows one to measure the structural phase \mathbf{d} in a diffraction experiment.

(3) **Polarization mixing:** For non-coplanar multiple-beam diffraction cases, i.e. \mathbf{L} not in the plane defined by \mathbf{H} and \mathbf{k}_0 , there is in general a mixing of the \mathbf{s} and \mathbf{p} polarization states in the detoured wave (Shen, 1991; 1993). This means that if the incident beam is purely \mathbf{s} -polarized, the diffracted beam may contain a \mathbf{p} -polarized component in the case of multiple-beam diffraction, which does not happen in the case of two-beam diffraction. It can be shown that the polarization properties of the detour-diffracted beam in a 3-beam case is governed by the following 2x2 matrix:

$$\underline{\mathbf{A}} = \begin{pmatrix} k_L^2 - (\mathbf{L} \cdot \mathbf{s}_0)^2 & -(\mathbf{L} \cdot \mathbf{s}_0)(\mathbf{L} \cdot \mathbf{p}_0) \\ -(\mathbf{k}_L \cdot \mathbf{p}_H)(\mathbf{L} \cdot \mathbf{s}_0) & k_L^2(\mathbf{p}_H \cdot \mathbf{p}_0) - (\mathbf{k}_L \cdot \mathbf{p}_H)(\mathbf{L} \cdot \mathbf{p}_0) \end{pmatrix}.$$

The off-diagonal elements in $\underline{\mathbf{A}}$ indicate the mixing of the polarization states.

The polarization mixing, together with the phase-sensitive multiple-beam interference, provides an unusual coupling to the incident beam polarization state, especially when the incident polarization contains a circularly polarized component. The effect has been used to extract acentric phase information and to determine noncentrosymmetry in quasicrystals (Shen & Finkelstein, 1990; Zhang et al. 1997). Using a known noncentrosymmetric crystal such as GaAs, the same effect provides a way to measure the degree of circular polarization and can be used to determine all Stokes polarization parameters for an x-ray beam (Shen & Finkelstein, 1992; 1993; Shen, Shastri & Finkelstein, 1995).

(4) *Multiple-beam standing waves*: The internal field in the case of multiple-beam diffraction is a three-dimensional standing wave. This 3-D standing wave can be detected, just like in the two-beam case, by observing x-ray fluorescence signals (Greiser & Matlik, 1986), and can be used to determine the 3-D location of the fluorescing atom similar to the method of triangulation by using multiple separate two-beam cases. Multiple-beam standing waves are also responsible for the so-called super-Borrmann effect because of additional lowering of the wave field intensity around the atomic planes (Borrmann & Hartwig, 1965).

Polarization Density Matrix

If the incident beam is partially polarized, i.e. it includes an unpolarized component, calculations in the case of multiple-beam diffraction can be rather complicated. One can simplify the algorithm a great deal by using a polarization *density matrix* as in the case of magnetic x-ray scattering (Blume & Gibbs, 1988). A polarization matrix is defined by

$$\underline{\mathbf{r}} = \frac{1}{2} \begin{pmatrix} 1 + P_1 & P_2 - iP_3 \\ P_2 + iP_3 & 1 - P_1 \end{pmatrix},$$

where (P_1, P_2, P_3) are the normalized Stokes-Poincare polarization parameters (Born & Wolf, 1983) that characterize the \mathbf{s} and \mathbf{p} linear polarization, $\pm 45^\circ$ tilted linear polarization, and left- and right-handed circular polarization, respectively.

A polarization-dependent scattering process, where the incident beam $(D_{0\sigma}, D_{0\pi})$ is scattered into $(D_{H\sigma}, D_{H\pi})$, can be described by a 2×2 matrix $\underline{\mathbf{M}}$ whose elements $M_{\sigma\sigma}$, $M_{\sigma\pi}$, $M_{\pi\sigma}$ and $M_{\pi\pi}$ represent the respective $\mathbf{s} \Rightarrow \mathbf{s}$, $\mathbf{s} \Rightarrow \mathbf{p}$, $\mathbf{p} \Rightarrow \mathbf{s}$, and $\mathbf{p} \Rightarrow \mathbf{p}$ scattering amplitudes:

$$\begin{pmatrix} D_{H\sigma} \\ D_{H\pi} \end{pmatrix} = \begin{pmatrix} M_{\sigma\sigma} & M_{\pi\sigma} \\ M_{\sigma\pi} & M_{\pi\pi} \end{pmatrix} \begin{pmatrix} D_{0\sigma} \\ D_{0\pi} \end{pmatrix}.$$

It can be shown that with the density matrix $\underline{\mathbf{r}}$ and scattering matrix $\underline{\mathbf{M}}$, the scattered new density matrix $\underline{\mathbf{r}}_H$

is given by $\underline{\mathbf{r}}_H = \underline{\mathbf{M}} \underline{\mathbf{r}} \underline{\mathbf{M}}^\dagger$, where $\underline{\mathbf{M}}^\dagger$ is the Hermitian conjugate of $\underline{\mathbf{M}}$. The scattered intensity I_H is obtained by calculating the trace of the new density matrix:

$$I_H = \text{Tr}(\underline{\mathbf{r}}_H).$$

This equation is valid for any incident beam polarization, including when the beam is partially polarized. We should note that the method is not restricted to dynamical theory and is widely used other physics fields such as quantum mechanics. In the case of multiple-beam diffraction, matrix $\underline{\mathbf{M}}$ can be evaluated using either the NBEAM program or one of the perturbation approaches.

V. GRAZING-ANGLE DIFFRACTION

Grazing incidence diffraction (GID) of x-rays or neutrons refers to situations where either the incident or the diffracted beams form a small angle less or around the critical angle of a well-defined crystal surface. In these cases both a Bragg diffracted beam *and* a specular reflected beam can occur simultaneously. Although there are only two beams, \mathbf{O} and \mathbf{H} , inside the crystal, the usual two-beam dynamical diffraction theory can not be applied to these situation without some modifications (Afanasyev & Melkonyan, 1983; Cowan et al. 1986; Hoche et al. 1986). These special considerations, however, can be automatically taken into account in the NBEAM theory discussed in the last Section, as shown by Durbin & Gog (1989).

A GID geometry may include the following situations: (i) specular reflection, (ii) coplanar grazing incident diffraction involving highly asymmetric Bragg reflections, and (iii) grazing incident diffraction in an inclined geometry. Because of the substantial decrease in the penetration depths of the incident beam in these geometries, there have been wide-spread applications of GID using synchrotron radiation in recent years in materials studies of surface structures (Marra, Eisenberger & Cho, 1979), depth-sensitive disorders and phase transitions (Dosch, 1992; Rhan et al. 1993; Rose et al., 1997; Krimmel et al., 1997), and long-period multilayers and superlattices (Barbee & Warberton, 1984; Salditt et al. 1994). We devote this section first to discuss the basic concepts in the GID geometries. A recent review on these topics has been given by Holy (1996). In the last segment of this section we present the principle of a distorted wave Born approximation (Vineyard, 1981; Dietrich & Wagner, 1983; 1984; Sinha et al. 1988), which provides a bridge between the dynamical Fresnel's formula and the kinematic theory of surface scattering of x-rays and neutrons.

Specular Reflectivity

It is straightforward to show that the Fresnel's optical reflectivity, which is widely used in studies of mirrors (e.g. Bilderback, 1981), can be recovered in the dynamical theory for x-ray diffraction. We recall that in the case of one-beam, the solution to the dispersion equation is given by Eq.(4). Assuming a semi-infinite crystal and using the general boundary condition Eqs.(7), we have the following equations across the interface:

$$\begin{aligned} D_0^i + D_0^e &= D_0 \\ k_0 \sin q (D_0^i - D_0^e) &= K_0 \sin q' D_0 \end{aligned}$$

where q and q' are the incident angles of the external and the internal incident beams (Fig.1b). Using Eq.(4) and the fact that \mathbf{K}_0 and \mathbf{k}_0 can differ only by a component normal to the surface, we arrive at the following wave field ratios (for small angles):

$$r_0 \equiv \frac{D_0^e}{D_0^i} = \frac{q - \sqrt{q^2 - q_c^2}}{q + \sqrt{q^2 - q_c^2}} \quad (38a)$$

$$t_0 \equiv \frac{D_0}{D_0^i} = \frac{2q}{q + \sqrt{q^2 - q_c^2}} \quad (38b)$$

with the critical angle defined as $q_c = (\Gamma F_0)^{1/2}$. For most materials q_c is on the orders of a few milliradians. In general, q_c can be complex in order to take into account absorption. Obviously Eqs.(38) gives the same reflection and transmission coefficients as the Fresnel's theory in visible optics (see, e.g. Jackson, 1975). The specular reflectivity R is given by the square of the magnitude of Eq.(38a): $R = |r_0|^2$, while $|t_0|^2$ of Eq.(38b) is the internal wave field intensity at the surface. An example of $|r_0|^2$ and $|t_0|^2$ is shown in Fig.9(a,b) for a GaAs surface.

At $q \gg q_c$, q in Eqs.(38) should be replaced by the original $\sin q$ and the Fresnel reflectivity $|r_0|^2$ varies as $1/(2\sin q)^4$, or as $1/q^4$ with q being the momentum transfer normal to the surface. This inverse-fourth-power law is the same as that derived in kinematic theory (Sinha et al. 1988) and in the theory of small-angle scattering (Porod, 1952; 1982). At first glance the $1/q^4$ asymptotic law is drastically different from the crystal truncation rod $1/q^2$ behavior for the Bragg reflection tails. A more careful inspection shows that the difference is due to the integral nature of the reflectivity over a more fundamental physical quantity called *differential cross-section*, $d\mathbf{s}/d\mathbf{W}$, which is defined as the incident flux scattered into a detector area that forms a solid angle $d\mathbf{W}$ with respect to the scattering source. In both Fresnel reflectivity and Bragg reflection cases, $d\mathbf{s}/d\mathbf{W} \sim 1/q^2$ in reciprocal space

units. Reflectivity calculations in both cases involve integrating over the solid angle and converting the incident flux into an incident intensity, each would give rise to a factor of $1/\sin q$ (Sinha et al. 1988). The only difference now is that in the case of Bragg reflections, this factor is simply $1/\sin q_B$, which is a constant for a given Bragg reflection, whereas for Fresnel reflectivity cases $\sin q \sim q$ resulting in an additional factor of $1/q^2$.

Evanescient Wave

When $q < q_c$, the normal component K_{0n} of the internal wavevector \mathbf{K}_0 is imaginary so that the x-ray wavefield inside the material diminishes exponentially as a function of depth, as given by

$$\mathbf{D}_0(\mathbf{r}) = t_0 e^{-\text{Im}(K_{0n})r_n} e^{-ik \cdot \mathbf{r}_t}, \quad (39)$$

where t_0 is given by Eq.(38b) and r_n and \mathbf{r}_t are the respective coordinates normal and parallel to the surface.

The characteristic penetration depth t ($1/e$ value of the intensity) is given by $t = 1/[2\text{Im}(K_{0n})]$. A plot of t as function of incident angle q is shown in Fig.9(c). In

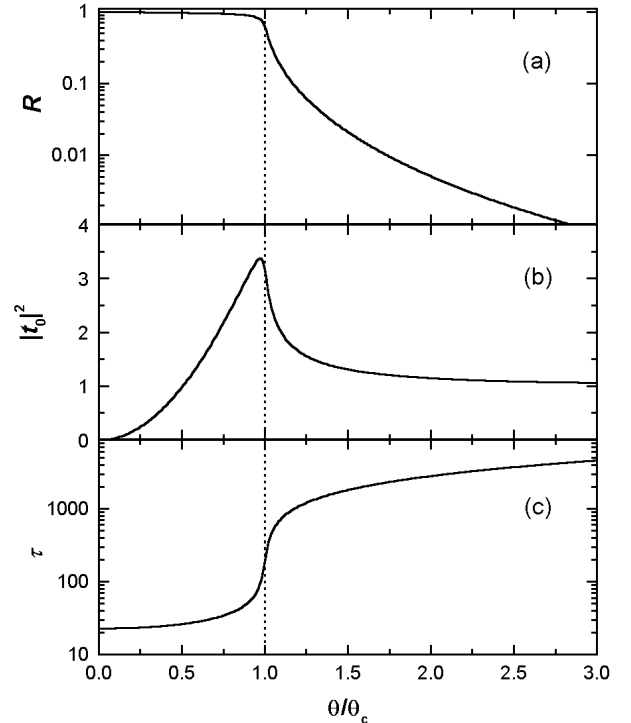


Figure 9: (a) Fresnel's reflectivity curve for a GaAs surface at 1.48 Angstroms. (b) Intensity of the internal field at the surface. (c) Penetration depth in Angstroms.

general, a penetration depth (known as *skin depth*) as short as 10-30 Å can be achieved with Fresnel's specular reflection when $q < q_c$. The limit at $q=0$ is simply given by $t=1/(4\pi q)$ with l being the x-ray wavelength. This makes the x-ray reflectivity-related measurement a very useful tool for studying surfaces of various materials.

At $q > q_c$ t becomes quickly dominated by true photoelectric absorption and the variation is simply geometrical. The large variation of t around $q \sim q_c$ forms the basis for such depth-controlled techniques as x-ray fluorescence under total external reflection (de Boer, 1991; Hoogenhof & de Boer, 1994), grazing-incidence scattering and diffraction (Dosch, 1992; Lied et al. 1994; Dietrich & Hasse, 1995; Gunther et al. 1997), and grazing-incidence x-ray standing-waves (Jach et al. 1989; Hashizume & Sakata, 1989; Jach & Bedzyk, 1993).

Multilayers and Superlattices

Synthetic multilayers and superlattices usually have long periods of 20-50 Å. Since the Bragg angles corresponding to these periods are necessarily small in an ordinary x-ray diffraction experiment, the superlattice diffraction peaks are usually observed in the vicinity of specular reflections. Thus dynamical theory is often needed to describe the diffraction patterns from multilayers of amorphous materials and superlattices of nearly perfect crystals.

A computational method to calculate the reflectivity from a multilayer system was first developed by Parratt (1954). In this method, a series of recursive equations on the wave field amplitudes is set up, based on the boundary conditions at each interface. Assuming that the last layer is a substrate that is sufficiently thick, one can find the solution of each layer backwards and finally obtain the reflectivity from the top layer. For details of this method we refer the readers to Parratt's original paper (1954) and to a more recent matrix formalism reviewed by Holy (1996).

It should be pointed out that near the specular region, the internal crystalline structures of the superlattice layers can be neglected, and only the average density of each layer would contribute. Thus the reflectivity calculations for multilayers and for superlattices are identical near the specular reflections. The crystalline nature of a superlattice needs to be taken into account near or at Bragg reflections. With the help of Takagi-Taupin equations, lattice mismatch and variations along the growth direction can also be taken into account, as shown by Bartels, Hornstra, and Lobeek (1986). By treating a semi-infinite single crystal as an extreme case of a superlattice or multilayer, one can calculate the reflectivity for the entire range from specular to all of the Bragg reflections along a given crystallographic axis (Caticha, 1994).

X-ray diffraction studies of laterally structured superlattices with periods of $\sim 0.1-1 \mu\text{m}$, such as surface gratings and quantum wire and dot arrays, have been of much interests in the materials society in recent years (Bauer et al. 1996; Shen, 1996). Most of these studies can be dealt with using kinematic diffraction theory (Aristov et al., 1986), and a rich amount of information can be obtained such as feature profiles (Shen et al., 1993; Darhuber et al., 1994), roughness on side wall surfaces (Darhuber et al., 1994), imperfections in grating arrays (Shen et al., 1996), size-dependent strain fields (Shen et al., 1996), and strain gradients near the interfaces (Shen & Kycia, 1997). Only in the regimes of total external reflection and grazing incidence diffraction, dynamical treatments are necessary as demonstrated by Tolan et al. (1992, 1995) and by Darowski et al. (1997).

Grazing Incidence Diffraction

Since most grazing incidence diffraction experiments are performed in the inclined geometry, we will focus only on this geometry and refer the highly asymmetric cases to the literature (Hoche et al., 1988; Kimura & Harada, 1994; Holy, 1996).

In an inclined grazing incidence diffraction arrangement, both the incident beam and the diffracted beam form a small angle with respect to the surface, as shown in Fig.10(a), with the scattering vector parallel to the surface. This geometry involves two internal waves \mathbf{O} and \mathbf{H} , and three external, incident \mathbf{O} , specular reflected $\overline{\mathbf{O}}$, and diffracted \mathbf{H} , beams. With proper boundary conditions, the diffraction problem can be solved analytically as shown by several authors (Afanasev & Melkonyan, 1983; Cowan et al., 1986; Hoche et al. 1986; Hung & Chang, 1989; Jach et al. 1989). Durbin and Gog (1989) have applied the NBEAM program to the GID geometry.

A characteristic dynamical effect in the GID geometry is a double-critical-angle phenomenon due to the diameter gap of the dispersion surface for the \mathbf{H} -reflection. This can be seen intuitively from simple geometric considerations. Inside the crystal, only two beams, \mathbf{O} and \mathbf{H} , are excited and thus the usual two-beam theory described in Section III applies. The dispersion surface inside the crystal is exactly the same as shown in Fig.2(a). The only difference is the boundary condition. In the GID case, the surface normal is *perpendicular* to the page in Fig.2 and therefore the circular curvature out of the page needs to be taken account. For simplicity we consider only the diameter points on the dispersion surface for one polarization state. A cut through the diameter points L and Q in Fig.2 is schematically shown in Fig.10(b), which consists of three concentric circles representing the revolutionary hyperboloids, α and β branches, and the vacuum sphere at point L . At very small incident angles, we see that no tie points can be

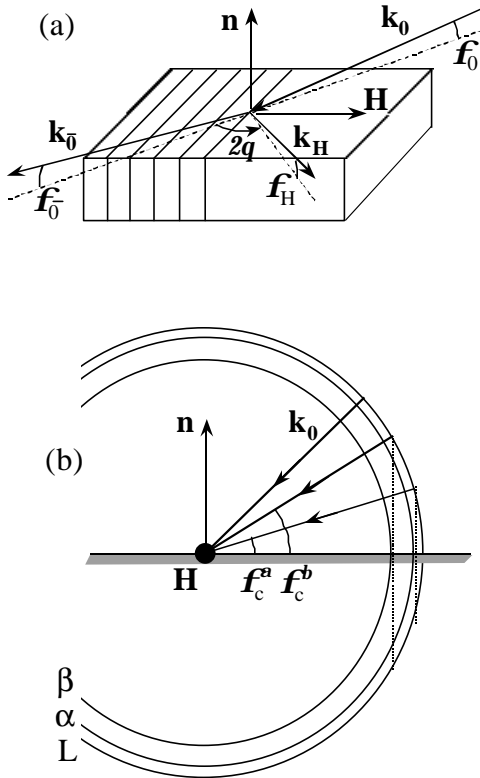


Figure 10: (a) Schematic of the grazing incidence diffraction geometry. (b) A cut through the diameter points of the dispersion surface.

excited and only total specular reflection can exist. As the incident angle increases so that $f > f_c^\alpha$, α tie points are excited but β -branch remains extinguished. Thus specular reflectivity would maintain a lower plateau, until $f > f_c^\beta$ when both α and β modes can exist inside the crystal. Meanwhile the Bragg reflected beam should have been fully excited when $f_c^\alpha < f < f_c^\beta$, but because of the partial specular reflection its diffracted intensity is much reduced. These effects can be clearly seen in the example shown in Fig.11 which is for a Ge(220) reflection with a (1-11) surface orientation.

If the Bragg's condition is not satisfied exactly, then the circle labeled L in Fig.10(b) would be split into two concentric ones representing the two spheres centered at \mathbf{O} and \mathbf{H} respectively. We then see that the exit take-off angles can be different for the reflected \mathbf{O} beam and the diffracted \mathbf{H} beam. With a position-sensitive linear detector and a range of incident angles, angular profiles (or rod-profiles) of diffracted beams can be observed directly, which can provide depth-sensitive structural

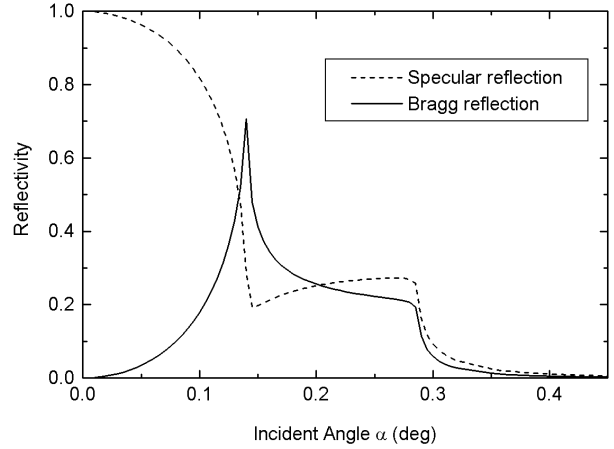


Figure 11: Specular and Bragg reflectivity at the center of the rocking curve for the Ge (220) reflection with a (1-11) surface orientation.

information near a crystal surface (Dosch et al. 1986, Bernhard et al. 1987).

Distorted-wave Born approximation

Grazing incident diffraction discussed in the last segment can be viewed as the dynamical diffraction of the internal evanescent wave, Eq.(39), generated by specular reflection under grazing angle conditions. If the rescattering mechanism is relatively weak, as in the case of a surface layer, then dynamical diffraction theory may not be necessary and the Born approximation can be substituted to evaluate the scattering of the evanescent wave. This approach is called the *distorted-wave Born approximation* (DWBA) in quantum mechanics (see, e.g. Schiff, 1968) and was first applied to x-ray scattering from surfaces by Vineyard (1982) and by Dietrich and Wagner (1983, 1984). It was noted by Dosch *et al.* (1986) that Vineyard's original treatment did not handle the exit-angle dependence properly because of a missing factor in its reciprocity arrangement.

The DWBA have been applied to several different scattering situations, including specular diffuse scattering from a rough surface, crystal truncation rod scattering near a surface, diffuse scattering in multilayers, and near-surface diffuse scattering in binary alloys. The underlying principle is the same for all these cases and we will only use the specular diffuse scattering to illustrate these principles.

From dynamical theory point of view, the DWBA is schematically shown in Fig.12(a). An incident beam \mathbf{k}_0

creates an internal incident beam \mathbf{K}_0 and a specular reflected beam $\mathbf{k}_{\bar{0}}$. We then assume that the internal beam \mathbf{K}_0 is scattered by a weak ‘‘Bragg reflection’’ at a lateral momentum transfer \mathbf{q}_t . Similar to the two-beam case in dynamical theory, we draw two spheres centered at \mathbf{q}_t shown as the dashed circles in Fig.12(a). However, the internal diffracted wavevector is determined by kinematic scattering as $\mathbf{K}_{\bar{q}} = \mathbf{K}_0 + \mathbf{q}$, where \mathbf{q} includes both the lateral component \mathbf{q}_t and a component \mathbf{q}_n normal to the surface defined by the usual $2\mathbf{q}$ angle. Therefore only one of the tie points on the internal sphere is excited, giving rise to $\mathbf{K}_{\bar{q}}$. Outside the surface, we have two tie points that yield \mathbf{k}_q and $\mathbf{k}_{\bar{q}}$ respectively, as defined in the dynamical theory. Altogether we have six beams, three associated with \mathbf{O} and three associated with \mathbf{q} . The connection between the \mathbf{O} -beams and the \mathbf{q} -beams is through the internal *kinematic* scattering:

$$\mathbf{D}_{\bar{q}} = S(\mathbf{q}_t) \mathbf{D}_0, \quad (40)$$

where $S(\mathbf{q}_t)$ is the surface scattering form factor. As will be seen later, $|S(\mathbf{q}_t)|^2$ represents the scattering cross-section per unit surface area defined by Sinha *et al.* (1988) and equals the Fourier transform of the height-height correlation function $C(\mathbf{r}_t)$ in the case of not-too-rough surfaces.

To find the diffuse-scattered exit wavefield $\mathbf{D}_{\bar{q}}^e$, we use the optical reciprocity theorem of Helmholtz (Born & Wolf, 1983) and reverse the directions of all three wavevectors of the \mathbf{q} -beams. We see immediately that the situation is identical to that discussed at the beginning of this Section for Fresnel reflections. Thus we should have that

$$\mathbf{D}_{\bar{q}}^e = t_q \mathbf{D}_{\bar{q}}^i, \quad t_q = \frac{2q_q}{q_q + \sqrt{q_q^2 - q_c^2}}.$$

Using Eq.(38b) and Eq.(40), we obtain that

$$\mathbf{D}_{\bar{q}}^e = t_0 t_q S(\mathbf{q}_t) \mathbf{D}_0^i$$

and the diffuse scattering intensity is simply given by

$$I_{diff} = \left| \mathbf{D}_{\bar{q}}^e / \mathbf{D}_0^i \right|^2 = |t_0|^2 |t_q|^2 |S(\mathbf{q}_t)|^2. \quad (41)$$

Apart from a proper normalization factor, Eq.(41) is the same as that given by Sinha *et al.* (1988). Of course here the scattering strength $|S(\mathbf{q}_t)|^2$ is only a symbolic quantity. For the physical meaning of various surface roughness correlation functions and its scattering forms, we refer to

the article by Sinha *et al.* (1988) for more a detailed discussion.

In a specular reflectivity measurement, one usually use the so-called rocking scans to record a diffuse scattering profile. The amount of the diffuse scattering is

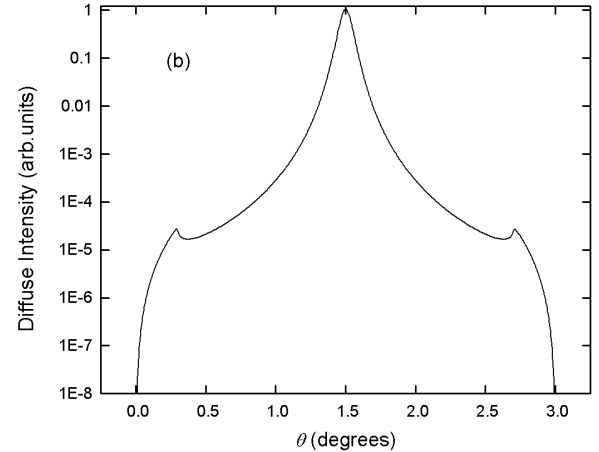
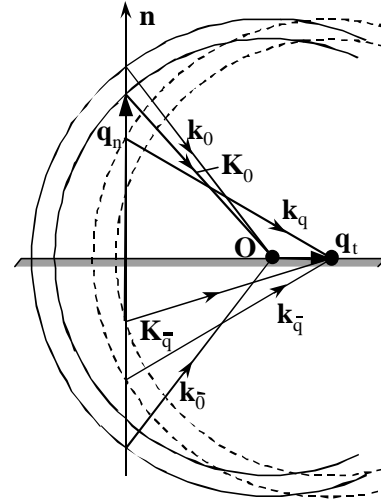
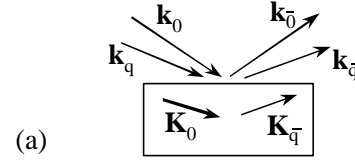


Figure 12: (a) Dynamical theory illustration of the distorted-wave Born approximation. (b) Typical diffuse scattering profile in specular reflectivity with Yoneda wings.

determined by the overall surface roughness and the shape of the profile is determined by the lateral roughness correlations. An example of computer-simulated rocking scan is shown in Fig.12(b) for a GaAs surface at 1.48 Å with the detector $2\mathbf{q}=3^\circ$. $|S(\mathbf{q}_\perp)|^2$ is assumed to be a Lorentzian with a correlation length of 4000 Å. The two peaks at $\mathbf{q}\sim 0.3^\circ$ and 2.7° correspond to the incident or the exit beam makes the critical angle with respect to the surface. These peaks are essentially due to the enhancement of the evanescent wave (standing wave) at the critical angle (Fig.9b) and are often called the Yoneda wings as they were first observed by Yoneda (1963).

Diffuse scattering of x-rays, neutrons and electrons is widely used in materials science to characterize surface morphology and roughness. The measurements can be performed not only near specular reflection but also around non-specular crystal truncation rods in glancing incidence inclined geometry (Shen et al., 1989; Stepanov, et al. 1996). Spatially correlated roughness and morphologies in multilayer systems have also been studied using diffuse x-ray scattering (Headrick & Baribeau, 1993; Baumbach et al. 1994; Paniago et al., 1996; Kaganer et al. 1996; Darhuber et al., 1997). Some of these topics are presented in detail in the previous Unit and in the Unit on x-ray surface scattering.

Expanded Distorted-Wave Approximation

The scheme of distorted-wave approximation can be extended to calculate nonspecular scattering that includes multilayer diffraction peaks from a multilayer system where a recursive Fresnel's theory is usually used to evaluate the distorted-wave (Kortright and Fischer-Colbrie, 1987; Holy and Baumbach, 1994). Recently Shen (1999b,c) has further developed an expanded distorted-wave approximation (EDWA) to include multiple-beam diffraction from bulk crystals where a two-beam dynamical theory is applied to obtain the distorted internal waves. In Shen's EDWA theory, a *sinusoidal* Fourier component \mathbf{G} is added to the distorting susceptibility component, which represents a charge-density modulation of the \mathbf{G} reflection. Instead of the Fresnel theory, a two-beam dynamical theory is employed to evaluate the distorted-wave, while the subsequent scattering of the distorted-wave is again handled by the first-order Born approximation. We now briefly outline this EDWA approach.

Following the formal distorted-wave description given in Vineyard (1982), $\mathbf{de}(\mathbf{r})$ in the fundamental equation (3) is separated into a distorting component $\mathbf{de}_1(\mathbf{r})$ and the remaining part $\mathbf{de}_2(\mathbf{r})$: $\mathbf{de}(\mathbf{r}) = \mathbf{de}_1(\mathbf{r}) + \mathbf{de}_2(\mathbf{r})$, where $\mathbf{de}_1(\mathbf{r})$ contains the homogeneous average susceptibility, *plus* a single predominant Fourier component \mathbf{G} :

$$\mathbf{de}_1(\mathbf{r}) = -\mathbf{G}(F_0 + F_G e^{-i\mathbf{G}\cdot\mathbf{r}} + F_{\bar{G}} e^{i\mathbf{G}\cdot\mathbf{r}}), \quad (76)$$

and the remaining $\mathbf{de}_2(\mathbf{r})$ is

$$\mathbf{de}_2(\mathbf{r}) = -\mathbf{G} \sum_{L \neq 0, \pm\mathbf{G}} F_L e^{-i\mathbf{L}\cdot\mathbf{r}}. \quad (77)$$

Since $F_G = |F_G| \exp(i\mathbf{a}_G)$ and $F_{\bar{G}} = F_G^* = |F_G| \exp(-i\mathbf{a}_G)$ if absorption is negligible, it can be seen that the additional component in Eq.(76) represents a sinusoidal distortion, $-2\mathbf{G}|F_G| \cos(\alpha_G - \mathbf{G}\cdot\mathbf{r})$.

The distorted wave $\mathbf{D}_1(\mathbf{r})$, due only to $\mathbf{de}_1(\mathbf{r})$, satisfies the following equation:

$$(\nabla^2 + k_0^2)\mathbf{D}_1 = -\nabla \times \nabla \times (\mathbf{de}_1 \mathbf{D}_1), \quad (78)$$

which is a standard two-beam case since only \mathbf{O} and \mathbf{G} Fourier components exist in $\mathbf{de}_1(\mathbf{r})$, and can therefore be solved by the two-beam dynamical theory (Batterman and Cole, 1964; Pinsker, 1978). It can be shown that the total distorted wave $\mathbf{D}_1(\mathbf{r})$ can be expressed as follows:

$$\mathbf{D}_1(\mathbf{r}) = \mathbf{D}_0 (r_0 e^{-i\mathbf{K}_0 \cdot \mathbf{r}} + r_G e^{i\mathbf{a}_G} e^{-i\mathbf{K}_G \cdot \mathbf{r}}), \quad (79)$$

where in semi-infinite Bragg case

$$\begin{cases} r_0 = 1 \\ r_G = -\sqrt{|b|} (\mathbf{h}_G \pm \sqrt{\mathbf{h}_G^2 - 1}) \end{cases}, \quad (80)$$

and in thin transparent Laue case

$$\begin{cases} r_0 = \cos(A\mathbf{h}_G) + i \sin(A\mathbf{h}_G) \\ r_G = i\sqrt{|b|} \sin(A\mathbf{h}_G)/\mathbf{h}_G \end{cases}, \quad (81)$$

Here standard notations in two-beam dynamical theory (Pages 2b.2.6-12) are used. It should be noted that the amplitudes of these distorted waves, given by Eqs.(80, 81), are slow varying functions of depth z through parameter A , since A is much smaller than $\mathbf{K}_0 \cdot \mathbf{r}$ or $\mathbf{K}_G \cdot \mathbf{r}$ by a factor of $\sim \mathbf{G}|F_G|$ which ranges from 10^{-5} - 10^{-6} for inorganic to 10^{-7} - 10^{-8} for protein crystals.

We now consider the re-scattering of the distorted-wave $\mathbf{D}_1(\mathbf{r})$, Eq.(79), by the remaining part of the susceptibility $\mathbf{de}_2(\mathbf{r})$ defined in Eq.(77). Using first-order Born approximation, the scattered wave field $\mathbf{D}(\mathbf{r})$ is given by

$$\mathbf{D}(\mathbf{r}) = \frac{e^{-ik_0 r}}{4\pi r} \int d\mathbf{r}' e^{i\mathbf{k}_0 \cdot \mathbf{r}'} \nabla \times \nabla \times [\mathbf{de}_2(\mathbf{r}') \mathbf{D}_1(\mathbf{r}')], \quad (82)$$

where \mathbf{u} is a unit vector and r is the distance from the sample to the observation point, and the integral is evaluated over the sample volume. The amplitudes r_0 and r_G can be factored out of the integral because of their much weaker spatial dependence than $\mathbf{K}_0 \cdot \mathbf{r}$ or $\mathbf{K}_G \cdot \mathbf{r}$ as mentioned above. The primary extinction effects in Bragg cases and the Pendellosung effects in Laue cases are taken into account by first evaluating intensity $I_H(z)$ scattered by a volume element at certain depth z and then

taking an average over z to obtain the final diffracted intensity.

It is worth noting that the distorted wave, Eq.(79), can be viewed as the new incident wave for the Born approximation Eq.(59), and it consists of two beams, \mathbf{K}_0 and \mathbf{K}_G . These two ‘incident’ beams can each produce its own diffraction pattern. If reflection \mathbf{H} satisfies the Bragg’s law, $k_0\mathbf{u} = \mathbf{K}_0 + \mathbf{H} \equiv \mathbf{K}_H$, and is excited by \mathbf{K}_0 , then there always exists a reflection $\mathbf{H}-\mathbf{G}$, excited by \mathbf{K}_G , such that the doubly-scattered wave travels along the same direction as \mathbf{K}_H since $\mathbf{K}_G + \mathbf{H} - \mathbf{G} = \mathbf{K}_H$. With this in mind and using the algebra given on Page 2b.2.16, it is easy to show that Eq.(82) gives rise to the following scattered wave:

$$\mathbf{D}_H = Nr_e \mathbf{u} \times (\mathbf{u} \times \mathbf{D}_0) \frac{e^{-ik_0 r}}{r} (F_H r_0 + F_{H-G} r_G e^{ia_G}). \quad (83)$$

Normalizing to the conventional first-order Born wavefield $\mathbf{D}_H^{(1)}$ defined by Eq.(61), Eq.(83) can be rewritten as

$$\mathbf{D}_H = \mathbf{D}_H^{(1)} (r_0 + |F_{H-G} / F_H| r_G e^{id}), \quad (84)$$

where $\mathbf{d} = \alpha_{H-G} + \alpha_G - \alpha_H$ is the invariant triplet phase widely-used in crystallography. Finally, the scattered intensity into the $\mathbf{k}_H = \mathbf{K}_H = k_0\mathbf{u}$ direction is given by

$I_H = (1/t) \int_0^t |\mathbf{D}_H|^2 dz$, which is averaged over thickness t of the crystal as discussed in the last paragraph. Numerical results show that the EDWA theory outlined here provides excellent agreements with the full n-beam dynamical calculations even at the center of a multiple reflection peak. For further information, we refer to Shen’s (1999b, 2000).

VI. SUMMARY

We have reviewed the basic elements of dynamical diffraction theory for perfect or nearly-perfect crystals. Although the eventual goal of obtaining structural information is the same, the dynamical approach is considerably different from that in kinematic theory. A key distinction is the inclusion of multiple scattering processes in the dynamical theory whereas the kinematic theory is based on a single scattering event.

We have mainly focused on the Ewald-von-Laue approach of the dynamical theory. There are four essential ingredients in this approach: (1) dispersion surfaces that determine the possible wave fields inside the material, (2) boundary conditions that relate the internal fields to outside incident and diffracted beams, (3) intensities of diffracted, reflected, and transmitted beams

that can be directly measured, and (4) internal wave field intensities that can be measured indirectly from signals of secondary excitations.

Because of the inter-connections of different beams due to multiple scattering, experimental techniques based on dynamical diffraction can often offer unique structural information. Such techniques include determination of impurity locations with x-ray standing waves, depth-profiling with glancing-incidence diffraction and fluorescence, and direct measurements of phases of structure factors with multiple-beam diffraction. These new and developing techniques have benefited substantially from the rapid growth of synchrotron radiation facilities around the world. With more and newer-generation facilities becoming available, we believe that dynamical diffraction study of various materials will continue to expand its territory and become more common and routine to materials scientists and engineers.

The author would like to thank Boris Batterman, Ernie Fontes, Ken Finkelstein, and Stefan Kycia for critical reading of this manuscript. This work is supported by the National Science Foundation through CHESS under grant number DMR-9311772.

VII. REFERENCES

- Afanasev, A.M., and Melkonyan, M.K. 1983. X-ray diffraction under specular reflection conditions. Ideal crystals. *Acta Crystallogr. A* 39:207.
- Aleksandrov, P.A., Afanasev, A.M., and Stepanov, S.A. 1984. Bragg-Laue diffraction in inclined geometry. *Phys. Stat. Solidi (A)* 86:143.
- Anderson, S.K., Golovchenko, J.A., and Mair, G. 1976. New application of x-ray standing wave fields to solid state physics. *Phys. Rev. Lett.* 37:1141.
- Andrews, S.R., and Cowley, R.A. 1985. *J. Phys. C* 18:6427-6439.
- Aristov, V.V., Winter, U., Nikilin, A. Yu., Redkin, S.V., Snigirev, A.A., Zaumseil, P., and Yunkin, V.A. 1988. Interference thickness oscillations of an x-ray wave on periodically profiled silicon. *Phys. Stat. Sol. (A)* 108:651-655.
- Authier, A. 1970. Ewald waves in theory and experiment, in *Advances in structure research by diffraction methods*, edited by Brill, R. and Mason, R. 3:1-51 (Pergamon Press, Oxford).
- Authier, A. 1986. Angular dependence of the absorption-induced nodal plane shifts of x-ray stationary waves. *Acta Crystallogr. A* 42:414-425.
- Authier, A. 1992. Dynamical theory of x-ray diffraction, in *International Tables of Crystallography*, ed. Shmueli, U., Academic Publishers, Dordrecht, vol.B:464-480.
- Authier, A. 1996. Dynamical theory of x-ray diffraction – I. Perfect crystals; II. Deformed crystals, in *X-ray and Neutron*

- Dynamical Diffraction: Theory and Applications*, eds. Authier, A., Lagomarsino, S. and Tanner, B.K., Plenum Press, New York.
- Barbee, T.W., and Warburton, W.K. 1984. X-ray evanescent and standing-wave fluorescence studies using a layered synthetic microstructure. *Mat. Lett.* 3:17.
- Bartels, W.J., Hornstra, J., and Lobeek, D.J.W. 1986. X-ray diffraction of multilayers and superlattices. *Acta Crystallogr. A* 42: 539:545.
- Batterman, B. W. 1969. Detection of foreign atom sites by their x-ray fluorescence scattering. *Physical Review Letters* 22:14.
- Batterman, B.W. 1964. Effect of dynamical diffraction in x-ray fluorescence scattering. *Phys. Rev.* 133:759.
- Batterman, B.W. 1992. X-ray phase plate. *Phys. Rev. B* 45:12677-12681.
- Batterman, B.W. and Cole, H. 1964. Dynamical diffraction of x-rays by perfect crystals. *Rev. Mod. Phys.* 36:681-717.
- Batterman, B.W., and Bilderback, D.H. 1991. X-ray monochromators and mirrors, in *Handbook on Synch. Rad.* edited by Brown, G.S. and Moncton, D.E. vol.3:105-153.
- Bauer, G., Darhuber, A.A., Holy, V. 1996. Structural characterization of reactive ion etched semiconductor nanostructures using x-ray reciprocal space mapping. *Mat. Res. Soc. Symp. Proc.* 405:359-370.
- Baumbach, G.T., Holy, V., Pietsch, U., Gailhanou, M. 1994. The influence of specular interface reflection on grazing incidence X-ray diffraction and diffuse scattering from superlattices. *Physica B* 198:249-52.
- Bedzyk, M.J. and Materlik, G. 1985. Two-beam dynamical solution of the phase problem: a determination with x-ray standing-wave fields. *Phys. Rev. B* 32:6456-6463.
- Bedzyk, M.J., Bilderback, D., White, J., Abruna, H.D., and Bommarito, M.G. 1986. Probing electrochemical interfaces with x-ray standing waves. *J. Phys. Chem.* 90:1926.
- Bedzyk, M.J., Bilderback, D.H., Bommarito, G.M., Caffrey, M., Schildkraut, J.S. 1988. Long-period standing waves as molecular yardstick. *Science* 241:1788-1791.
- Bedzyk, M.J., Shen, Q., Keeffe, M., Navrotsky, G., and Berman, L.E. 1989. X-ray standing wave surface structural determination for iodine on Ge (111). *Surf. Sci.* 220:419-427.
- Belyakov, V. and Dmitrienko, V. 1989. Polarization phenomena in x-ray optics. *Sov. Phys. Uspekhi.* 32:697-719.
- Berman, L.E., Batterman, B.W., and Blakely, J.M. 1988. Structure of submonolayer gold on silicon (111) from x-ray standing-wave triangulation. *Phys. Rev. B* 38:5397.
- Bernhard, N., Burkel, E., Gompper, G., Metzger, H., Peisl, J., Wagner, H., Wallner, G. 1987. Grazing incidence diffraction of X-rays at a Si single crystal surface: Comparison of theory and experiment. *Z. Physik B* 69:303-311.
- Bethe, H.A. 1928. ????. *Ann. Phys. Lpz.* 87:55.
- Bilderback, D.H. 1981. Reflectance of x-ray mirrors from 3.8 to 50 keV (3.3 to 0.25 Å). *SPIE Proceedings* 315:90-102.
- Bilderback, D.H., Hoffman, S.A., and Thiel, D.J. 1994. ????. *Science* 263:201-203.
- Blume, M. and Gibbs, D. 1988. *Phys. Rev. B* 37:1779-1789.
- Born, M. and Wolf, E. 1983. *Principles of Optics*, 6th ed., Pergamon, New York.
- Borrmann, G. 1950. Die absorption von Rontgenstrahlen in fall der interferenz. *Z. Phys.* 127:297-323.
- Borrmann, G. and Hartwig, Z. 1965. *Z. Krist.* 121:401.
- Brummer, O., Eisenschmidt, Ch., and Hoche, H. 1984. Polarization phenomena of x-rays in the Bragg case. *Acta Crystallogr. A* 40:394-398.
- Caticha, A. 1993. Diffraction of x-rays at the far tails of the Bragg peaks. *Phys. Rev. B* 47:76-83.
- Caticha, A. 1994. Diffraction of x-rays at the far tails of the Bragg peaks. II. Darwin dynamical theory. *Phys. Rev. B* 49:33-38.
- Chang, S.-L. 1998. Determination of X-ray Reflection Phases Using N-Beam Diffraction. *Acta Cryst. A* 54:886-894.
- Chang, S.L. 1982. Direct determination of x-ray reflection phases. *Phys. Rev. Lett.* 48:163-166.
- Chang, S.L. 1984. *Multiple Diffraction of X-rays in Crystals*. Springer Verlag, Berlin, Heidelberg, New York.
- Chang, S.L. 1992. X-ray phase problem and multi-beam interference. *Int. J. Mod. Phys.* 6:2987-3020.
- Chang, S.-L., Huang, Y.-S., Chao, C.-H., Tang, M.-T., and Stetsko, Y.P. 1998. Three-wave resonance grazing incidence x-ray diffraction: a novel method for direct phase determination of surface in-plane reflections. *Physical Review Letters* 80:301-304.
- Chang, S.-L., Chao, C.-H., Huang, Y. -S., Jean, Y. -C., Sheu, H. -S., Liang, F. -J., Chien, H. -C., Chen, C. -K., and Yuan, H. S. 1999. Quantitative phase determination for macromolecular crystals using stereoscopic multibeam imaging. *Acta Cryst. A* 55:933-938.
- Chang, S.L., King, H.E. Jr., Huang, M-T, and Gao, Y. 1991. Direct phase determination of large macromolecular crystals using three-beam x-ray interference. *Phys. Rev. Lett.* 67:3113-3116.
- Chapman, L.D., Yoder, D.R., and Colella, R. 1981. Virtual Bragg scattering: a practical solution to the phase problem. *Phys. Rev. Lett.* 46:1578-????.
- Chikawa, J-I. And Kuriyama, M. 1991. Topography, in *Handbook on Synch. Rad.* edited by Brown, G.S. and Moncton, D.E. vol.3:337-378.
- Chung, Jin-Seok, Durbin, S.M. 1995. Dynamical diffraction in quasicrystals. *Physical Review B* 51:14976-9.
- Cole, H., Chambers, F.W., and Dunn, H.M. 1962. Simultaneous diffraction: indexing Umweganregung peaks in simple cases. *Acta Crystallogr.* 15:138-144.
- Colella, R. 1972. N-beam dynamical diffraction of high-energy electrons at glancing incidence. General theory and computational methods. *Acta Crystallogr. A* 28:11-15.
- Colella, R. 1974. Multiple diffraction of x-rays and the phase problem. computational procedures and comparison with experiment. *Acta Crystallogr. A* 30:413-423.

- Colella, R. 1991. Truncation rod scattering: analysis by dynamical theory of x-ray diffraction. *Phys. Rev. B* 43:13827.
- Colella, R. 1995. Multiple Bragg scattering and the phase problem in x-ray diffraction. I perfect crystals. *Comments Cond. Mat. Phys.* 17:175-215.
- Colella, R.. 1996. Multiple Bragg scattering and the phase problem in x-ray diffraction: Perfect crystals; Mosaic crystals, in *X-ray and Neutron Dynamical Diffraction: Theory and Applications*, eds. Authier, A., Lagomarsino, S. and Tanner, B.K., Plenum Press, New York.
- Cowan, P.L., Brennan, S., Jach, T., Bedzyk, M.J., and Materlik, G. 1986. *Phys. Rev. Lett.* 57:2399.
- Cowley, J.M. 1975. *Diffraction Physics*. North-Holland, Amsterdam.
- Darhuber, A.A., Koppensteiner, E., Straub, H., Brunthaler, G., Faschinger, W., Bauer, G. 1994. Triple axis x-ray investigations of semiconductor surface corrugations. *J. Appl. Phys.* 76:7816-7823.
- Darhuber, A.A., Schittenhelm, P., Holy, V., Stangl, J., Bauer, G., Abstreiter, G. 1997. High-resolution x-ray diffraction from multilayered self-assembled Ge dots. *Phys. Rev. B* 55:15652-15663.
- Darowski, N., Paschke, K., Pietsch, U., Wang, K.H., Forchel, A., Baumbach, T., Zeimer, U. 1997. Identification of a buried single quantum well within surface structured semiconductors using depth resolved x-ray grazing incidence diffraction. *J. Phys. D* 30:L55-L59.
- Darwin, C.G. 1922. The reflection of x-rays from imperfect crystals. *Phil. Mag.* 43:800-829.
- Darwin, C.G. 1914. The theory of x-ray reflexion. *Phil. Mag.* 27:315-333; 27:675-690.
- De Boer, D.K.G. 1991. Glancing-incidence X-ray fluorescence of layered materials. *Physical Review B* 44:498-511.
- Dietrich, S. and Wagner, H. 1983. Critical surface scattering of x-rays and neutrons at grazing angles. *Phys. Rev. Lett.* 51:1469.
- Dietrich, S. and Wagner, H. 1984. *Z. Phys. B* 56:207.
- Dietrich, S., Haase, A. 1995. Scattering of X-rays and neutrons at interfaces. *Physics Reports* 260:1-138.
- Dosch, H. 1992. Evanescent X-rays probing surface-dominated phase transitions. *International Journal of Modern Physics B* 6:2773-2808.
- Dosch, H., Batterman, B. W. and Wack, D. C. 1986. Depth-controlled grazing-incidence diffraction of synchrotron x-radiation. *Physical Review Letters* 56:1144.
- Durbin, S. M., Berman, L. E., Batterman, B. W. and Blakely, J. M. 1986. Measurement of the silicon (111) surface contraction. *Physical Review Letters* 56:236.
- Durbin, S.M. 1987. Dynamical diffraction of x-rays by perfect magnetic crystals. *Phys. Rev. B* 36:639-643.
- Durbin, S.M. 1995. Darwin spherical-wave theory of kinematic surface diffraction. *Acta Crystallogr. A* 51:258-268.
- Durbin, S.M., and Gog, T. 1989. Bragg-Laue diffraction at glancing incidence. *Acta Crystallogr. A* 45:132-141.
- Durbin, S.M.; Follis, G.C. 1995. Darwin theory of heterostructure diffraction. *Phys. Rev. B* 51:10127-33.
- Durbin, S.M. 1988. X-ray standing wave determination of Mn sublattice occupancy in a $Cd_{1-x}Mn_xTe$ mosaic crystal. *J. Appl. Phys.* 64:2312-2315.
- Ewald, P.P. 1917. Zur Begründung der Kristallographie. III. Die Kristallographie der Röntgenstrahlen. *Ann. Physik (Leipzig)* 54:519-597.
- Ewald, P.P. and Heno, Y. 1968. X-ray diffraction in the case of three strong rays. I. Crystal composed of non-absorbing point atoms. *Acta Crystallogr. A* 24:5-15.
- Feng, Y.P., Sinha, S.K., Fullerton, E.E., Grubel, G., Abernathy, D., Siddons, D.P., and Hastings, J.B. 1995. X-ray Fraunhofer diffraction patterns from a thin-film waveguide. *Appl. Phys. Lett.* 67:3647.
- Fewster, P.F. 1996. Superlattices, in *X-ray and Neutron Dynamical Diffraction: Theory and Applications*, eds. Authier, A., Lagomarsino, S. and Tanner, B.K., Plenum Press, New York.
- Fontes, E., Patel, J.R., and Comin, F. 1993. Direct measurement of the asymmetric dimer buckling of Ge on Si (001). *Phys. Rev. Lett.* 70:2790-2793.
- Franklin, G.E., Bedzyk, M.J., Woicik, J.C., Chien Liu, Patel, J.R., Golovchenko, J.A. 1995. Order-to-disorder phase-transition study of Pb on Ge(111). *Phys. Rev. B* 51:2440-2445.
- Funke, P., and Materlik, G. 1985. *Solid State Commun.* 54:921.
- Giles, C., Malmange, C., Goulon, J., de Bergivin, F., Vettier, C., Dartyge, E., Fontaine, A., Giorgetti, C., and Pizzini, S. 1994. Energy-dispersive phase plate for magnetic circular dichroism experiments in the x-ray range. *J. Appl. Cryst.* 27:232-240.
- Golovchenko, J.A., Batterman, B.W., Brown, W.L. 1974. Observation of internal x-ray wave field during Bragg diffraction with an application to impurity lattice location. *Phys. Rev. B* 10:4239.
- Golovchenko, J.A., Kincaid, B.M., Levesque, R.A., Meixner, A.E., and Kaplan, D.R. 1986. Polarization Pendellosung and the generation of circularly polarized x-rays with a quarter-wave plate. *Phys. Rev. Lett.* 57:202-205.
- Golovchenko, J.A., Patel, J.R., Kaplan, D.R., Cowan, P.L., and Bedzyk, M.J. 1982. Solution to the surface registration problem using x-ray standing waves. *Phys. Rev. Lett.* 49:560.
- Greiser, N. and Materlik, G. 1986. Three-beam x-ray standing wave analysis: a two-dimensional determination of atomic positions. *Z. Phys. B* 66:83-89.
- Gunther, R., Odenbach, S., Scharpf, O., Dosch, H. 1997. Reflectivity and evanescent diffraction of polarized neutrons from Ni(110). *Physica B* 234-236:508-509.
- Hart, M. 1978. X-ray polarization phenomena. *Phil. Mag.* B 38:41-56.
- Hart, M. 1991. Polarizing x-ray optics for synchrotron radiation. *SPIE Proceedings* 1548:46-55.

- Hart, M. 1996. X-ray optical beamline design principles, in *X-ray and Neutron Dynamical Diffraction: Theory and Applications*, eds. Authier, A., Lagomarsino, S. and Tanner, B.K., Plenum Press, New York.
- Hashizume, H., Sakata, O. 1989. Dynamical diffraction of X-rays from crystals under grazing- incidence conditions. *Journal of the Crystallographic Society of Japan* 31:249-255; *Colloque de Physique C* 7:225-229.
- Headrick, R.L., Baribeau, J.M. 1993. Correlated roughness in Ge/Si superlattices on Si (100). *Phys. Rev. B* 48:9174-9177.
- Hirano, K., Ishikawa, T., and Kikuta, S. 1995. Development and application of x-ray phase retarders. *Rev. Sci. Instrum.* 66:1604-1609.
- Hirano, K., Izumi, K., Ishikawa, T., Annaka, S., and Kikuta, S. 1991. An x-ray phase plate using Bragg case diffraction. *Jpn. J. Appl. Phys.* 30:L407-L410.
- Hoche, H.R., Brummer, O., and Nieber, J. 1986. Extremely skew x-ray diffraction. *Acta crystallogr. A* 42:585-586.
- Hoche, H.R., Nieber, J., Clausnitzer, M., and Materlik, G. 1988. Modification of specularly reflected x-ray intensity by grazing incidence coplanar Bragg-case diffraction. *Phys. Stat. Solidi (A)* 105:33.
- Hoier, R. and Marthinsen, K. 1983. Effective structure factors in many-beam x-ray diffraction – use of the second Bethe approximation. *Acta Crystallogr. A* 39:854-860.
- Holy, V. 1996. Dynamical theory of highly asymmetric x-ray diffraction, in *X-ray and Neutron Dynamical Diffraction: Theory and Applications*, eds. Authier, A., Lagomarsino, S. and Tanner, B.K., Plenum Press, New York.
- Holy, V. and Baumbach, T. 1994. Nonspecular x-ray reflection from rough multilayers. *Phys. Rev. B* 49:10668-10676.
- Hoogenhof, W.W.V.D., de Boer, D.K.G. 1994. GIXA (Glancing Incidence X-ray Analysis), a novel technique in near-surface analysis. *Mater. Sci. Forum (Switzerland)* 143-147:1331-1335.
- Hummer, K., and Billy, H. 1986. Experimental determination of triplet phases and enantiomorphs of non-centrosymmetric structures. I. Theoretical considerations. *Acta Crystallogr. A* 42:127-133.
- Hummer, K., Schwegle, W., and Weckert, E. 1991. A feasibility study of experimental triplet-phase determination in small proteins. *Acta Crystallogr. A* 47:60-62.
- Hummer, K., Weckert, E., and Bondza, H. 1990. Direct measurements of triplet phases and enantiomorphs of non-centrosymmetric structures. experimental results. *Acta Crystallogr. A* 45:182-187.
- Hung, H.H., and Chang, S.L. 1989. Theoretical considerations on two-beam and multi-beam grazing-incidence x-ray diffraction: nonabsorbing cases. *Acta Crystallogr. A* 45:823-833.
- Jach, T., Bedzyk, M.J. 1993. X-ray standing waves at grazing angles. *Acta Crystallographica Section A* 49:346-350.
- Jach, T., Cowan, P.L., Shen, Q., and Bedzyk, M.J. 1989. Dynamical diffraction of x-rays at grazing angle. *Phys. Rev. B* 39:5739-5747.
- Jach, T., Zhang, Y., Colella, R., de Boissieu, M., Boudard, M., Goldman, A.I., Lograsso, T.A., Delaney, D.W., and Kycia, S. 1997. Dynamical diffraction and x-ray standing waves from 2-fold reflections of the quasicrystal AlPdMn. *Phys. Rev. Lett.*
- Jackson, J.D. 1974. *Classical Electrodynamics*. 2nd ed., John Wiley, New York.
- James, R.W. 1950. *The Optical Principles of the Diffraction of X-rays*. G. Bell and Sons Ltd., London.
- Juretschke, J.J. 1982. Invariant-phase information of x-ray structure factors in the two-beam Bragg intensity near a three-beam point. *Phys. Rev. Lett.* 48:1487-1489.
- Juretschke, J.J. 1984. Modified two-beam description of x-ray fields and intensities near a three-beam diffraction point. General formulation and first-order solution. *Acta Crystallogr. A* 40:379-389.
- Juretschke, J.J. 1986. Modified two-beam description of x-ray fields and intensities near a three-beam diffraction point. Second-order solution. *Acta Crystallogr. A* 42:449-456.
- Kaganer, V.M., Stepanov, S.A., Koehler, R. 1996. Effect of roughness correlations in multilayers on Bragg peaks in X-ray diffuse scattering. *Physica B* 221:34-43.
- Kato, N. 1952. Dynamical theory of electron diffraction for a finite polyhedral crystal. *J. Phys. Soc. Japan* 7:397-414.
- Kato, N. 1960. The energy flow of x-rays in an ideally perfect crystal: comparison between theory and experiments. *Acta Crystallogr.* 13:349-356.
- Kato, N. 1974. X-ray diffraction, in *X-ray Diffraction*, edited by Azaroff, L.V., Kaplow, R., Kato, N., Weiss, R.J., Wilson, A.J.C., and Young, R.A., McGraw-Hill, New York, 176-438.
- Kikuchi, S. 1928. *Proc. Jap. Acad. Sci.* 4:271.
- Kimura, S., and Harada, J. 1994. Comparison between experimental and theoretical rocking curves in extremely asymmetric Bragg cases of x-ray diffraction. *Acta Crystallogr. A* 50:337.
- Klapper, H. 1996. X-ray diffraction topography: application to crystal growth and plastic deformation, in *X-ray and Neutron Dynamical Diffraction: Theory and Applications*, eds. Authier, A., Lagomarsino, S. and Tanner, B.K., Plenum Press, New York.
- Kortright, J.B., Fischer-Colbrie, A. 1987. Standing wave enhanced scattering in multilayer structures. *J. Appl. Phys.* 61:1130-1133.
- Kossel, W., Loeck, V., and Voges, H. 1935. ????. *Z. Phys.* 94:139.
- Kovalchuk, M.V. and Kohn, V.G. 1986. X-ray standing wave – a new method of studying the structure of crystals. *Sol. Phys. Usp.* 29:426.
- Krimmel, S.; Donner, W.; Nickel, B.; Dosch, H.; Sutter, C.; Grubel, G. 1997. Surface segregation-induced critical phenomena at FeCo(001) surfaces. *Phys. Rev. Lett.* 78:3880-3883.
- Kycia, S.W., Goldman, A.I., Lograsso, T.A., Delaney, D.W., Black, D., Sutton, M., Dufresne, E., Bruning, R., Rodricks,

- B. 1993. Dynamical x-ray diffraction from an icosahedral quasicrystal. *Phys. Rev. B* 48:3544-3547.
- Lagomarsino, S. 1996. X-ray standing wave studies of bulk crystals, thin films and interfaces, in *X-ray and Neutron Dynamical Diffraction: Theory and Applications*, eds. Authier, A., Lagomarsino, S. and Tanner, B.K., Plenum Press, New York.
- Lagomarsino, S., Scarinci, F., and Tucciarone, A. 1984. X-ray standing waves in garnet crystals. *Phys. Rev. B* 29:4859.
- Lang, J.C.; Srajer, G.; Detlefs, C.; Goldman, A.I.; Konig, H.; Xindong Wang; Harmon, B.N.; McCallum, R.W. 1995. Confirmation of quadrupolar transitions in circular magnetic X-ray dichroism at the dysprosium L_{III} edge. *Phys. Rev. Lett.* 74:4935-4938
- Laue, M. von. 1931. Die dynamische theorie der Rontgenstrahlinterferenzen in neuer form. *Ergeb. Exakt. Naturwiss.* 10:133-158.
- Lee, H. and Colella, R. 1993. Phase determination of x-ray reflections in a quasicrystal. *Acta Crystallogr. A* 49:600-???
- Lied, A., Dosch, H., Bilgram, J.H. 1994: Glancing angle X-ray scattering from single crystal ice surfaces. *Physica B* 198:92-96.
- Lipcomb, W.N. 1949. Relative phases of diffraction maxima by multiple reflection. *Acta Crystallogr.* 2:193-194.
- Lyman, P.F.; Bedzyk, M.J. 1997. Local structure of Sn/Si(001) surface phases. *Surface Science* 371:307-315.
- Malgrange, C. 1996. X-ray polarization and applications, in *X-ray and Neutron Dynamical Diffraction: Theory and Applications*, eds. Authier, A., Lagomarsino, S. and Tanner, B.K., Plenum Press, New York.
- Marra, W.L., Eisenberger, P., and Cho, A.Y. 1979. ????. *J. Appl. Phys.* 50:6927.
- Martines, R.E., Fontes, E., Golovchenko, J.A., and Patel, J.R. 1992. Giant vibrations of impurity atoms on a crystal surface. *Phys. Rev. Lett.* 69:1061.
- Mills, D.M. 1988. Phase-plate performance for the production of circularly polarized x-rays. *Nucl. Instrum. Meth. A* 266:531-537.
- Moon, R.M. and Shull, C.G. 1964. The effects of simultaneous reflection on single-crystal neutron diffraction intensities. *Acta Crystallogr. A* 17:805-812
- Paniago, R., Homma, H., Chow, P.C., Reichert, H., Moss, S.C., Barnea, Z., Parkin, S.S.P., Cookson, D. 1996. Interfacial roughness of partially correlated metallic multilayers studied by nonspecular X-ray reflectivity. *Physica B* 221:10-12.
- Parrat, P.G. 1954. Surface studies of solids by total reflection of x-rays. *Phys. Rev.* 95:359-369.
- Patel, J.R. 1996. X-ray standing waves, in *X-ray and Neutron Dynamical Diffraction: Theory and Applications*, eds. Authier, A., Lagomarsino, S. and Tanner, B.K., Plenum Press, New York.
- Patel, J.R., Golovchenko, J.A., Freeland, P.E., and Gossmann, H-J. 1987. Arsenic atom location on passivated silicon (111) surfaces. *Phys. Rev. B* 36:7715.
- Pinsker, Z.G. 1978. *Dynamical scattering of x-rays in crystals*. Springer Series in Solid-State Sciences, Springer Verlag, Berlin.
- Porod, G. 1952. *Kolloid. Z.* 125:51-57; 108-122.
- Porod, G. 1982. In *Small Angle X-ray Scattering*, edited by Glatter, O. and Kratky, O. (Academic, New York).
- Post, B. 1977. Solution of the x-ray phase problem. *Phys. Rev. Lett.* 39:760-763.
- Prins, J.A. 1930. Die reflexion von Rontgenstrahlen an absorbierenden idealen kristallen. *Z. Physik* 63:477-493.
- Renninger, M. 1937. Umweganregung, eine bisher unbeachtete Wechselwirkungserscheinung bei Raumgitter-interferenzen. *Z. Physik.* 106:141-176.
- Rhan, H., Pietsch, U., Rugel, S., Metzger, H., Peisl, J. 1993. Investigations of semiconductor superlattices by depth-sensitive X-ray methods. *J. Appl. Phys.* 74:146-152.
- Robinson, I.K. Crystal truncation rods and surface roughness. *Phys. Rev. B* 33:3830-3836.
- Rose, D., Pietsch, U., Zeimer, U. 1997. Characterization of $In_xGa_{1-x}As$ single quantum wells, buried in GaAs[001], by grazing incidence diffraction. *Journal of Applied Physics* 81:2601-2606.
- Salditt, T., Metzger, T.H., and Peisl, J. 1994. Kinetic roughness of amorphous multilayers studied by diffuse x-ray scattering. *Phys. Rev. Lett.* 73:????.
- Schiff, L.I. 1955. *Quantum Mechanics*. 2nd ed. (McGraw-Hill, New York).
- Schlenker, M., and Guigay, J-P. 1996. Dynamical theory of neutron scattering, in *X-ray and Neutron Dynamical Diffraction: Theory and Applications*, eds. Authier, A., Lagomarsino, S. and Tanner, B.K., Plenum Press, New York.
- Schmidt, M.C. and Colella, R. 1985. Phase determination of forbidden x-ray reflections in V_3Si by virtual Bragg scattering. *Phys. Rev. Lett.* 55:715-718.
- Shastri, S.D., Finkelstein, K.D., Shen, Q., Batterman, B.W., and Walko, D.A. 1995. Undulator test of a Bragg-reflection elliptical polarizer at 7.1 keV. *Rev. Sci. Instrum.* 66:1581.
- Shen, Q. 1986. A new approach to multi-beam x-ray diffraction using perturbation theory of scattering. *Acta Crystallogr. A* 42:525-533.
- Shen, Q. 1991. Polarization state mixing in multiple beam diffraction and its application to solving the phase problem. *SPIE Proceedings* 1550:27-33.
- Shen, Q. 1993. Effects of a general x-ray polarization in multiple-beam Bragg diffraction. *Acta Crystallogr. A* 49:605-613.
- Shen, Q. 1996. Polarization Optics for High-Brightness Synchrotron X-rays. *SPIE Proceedings* 2856:82.
- Shen, Q. 1996. Study of periodic surface nanostructures using coherent grating x-ray diffraction (CGXD). *Mat. Res. Soc. Symp. Proc.* 405:371-379.
- Shen, Q. 1998. Solving the phase problem using reference-beam x-ray diffraction. *Phys. Rev. Lett.* 80:3268-3271.

- Shen, Q. 1999a. Direct measurements of Bragg-reflection phases in x-ray crystallography. *Phys. Rev. B* 59:11109-11112.
- Shen, Q. 1999b. Expanded distorted-wave theory for phase-sensitive x-ray diffraction in single crystals. *Phys. Rev. Lett.* Vol.83, in press, Dec. 6, 1999.
- Shen, Q. 2000. A distorted-wave approach to reference-beam x-ray diffraction in transmission cases. *Phys. Rev. B* 61:5893.
- Shen, Q. and Colella, R. 1987. Solution of phase problem for crystallography at a wavelength of 3.5 Å. *Nature* 329:232-233.
- Shen, Q. and Colella, R. 1988. Phase observation in organic crystal benzil using 3.5 Å x-rays. *Acta Crystallogr. Sect. A* 44:17-21.
- Shen, Q. and Finkelstein, K.D. 1990. Solving the phase problem with multiple-beam diffraction and elliptically polarized x rays. *Phys. Rev. Lett.* 65:3337-3340.
- Shen, Q. and Finkelstein, K.D. 1992. Complete determination of x-ray polarization using multiple-beam Bragg diffraction. *Phys. Rev. B* 45:5075-5078.
- Shen, Q. and Finkelstein, K.D. 1993. A complete characterization of x-ray polarization state by combination of single and multiple Bragg reflections. *Rev. Sci. Instrum.* 64:3451-3456.
- Shen, Q., Blakely, J.M., Bedzyk, M.J., Finkelstein, K.D. 1989. Surface roughness and correlation length determined from x-ray-diffraction line-shape analysis on Ge (111). *Phys. Rev. B* 40:3480-3482.
- Shen, Q., Kycia, S. 1997. Determination of interfacial strain distribution in quantum-wire structures by synchrotron x-ray scattering. *Phys. Rev. B* 55:15791-15797.
- Shen, Q., Kycia, S.W., Schaff, W.J., Tentarelli, E.S., Eastman, L.F. 1996. X-ray diffraction study of size-dependent strain in quantum wire structures, *Phys. Rev. B* 54:16381-16384.
- Shen, Q., Shastri, S., and Finkelstein, K.D. 1995. Stokes polarimetry for x-rays using multiple-beam diffraction. *Rev. Sci. Instrum.* 66:1610-1613.
- Shen, Q., Umbach, C.C., Weselak, B., Blakely, J.M. 1993. X-ray diffraction from a coherently illuminated Si (001) grating surface, *Phys. Rev. B* 48:17967.
- Shen, Q., Umbach, C.C., Weselak, B., Blakely, J.M. 1996. Lateral correlation in mesoscopic on silicon (001) surface determined by grating x-ray diffuse scattering. *Phys. Rev. B* 53:R4237-4240.
- Sinha, S.K., Sirota, E.B., Garoff, S., and Stanley, H.B. 1988. X-ray and neutron scattering from rough surfaces. *Phys. Rev. B* 38:2297-2311.
- Stepanov, S.A., Kondrashkina, E.A., Schmidbauer, M., Kohler, R.; Pfeiffer, J.-U.; Jach, T., Souvorov, A.Yu. 1996. Diffuse scattering from interface roughness in grazing-incidence X-ray diffraction. *Phys. Rev. B* 54:8150-8162.
- Takagi, S. 1962. Dynamical theory of diffraction applicable to crystals with any kind of small distortion. *Acta Crystallogr.* 15:1311-1312.
- Takagi, S. 1969. A dynamical theory of diffraction for a distorted crystal. *J. Phys. Soc. Jap.* 26:1239-1253.
- Tanner, B.K. 1996. Contrast of defects in x-ray diffraction topographs, in *X-ray and Neutron Dynamical Diffraction: Theory and Applications*, eds. Authier, A., Lagomarsino, S. and Tanner, B.K., Plenum Press, New York.
- Taupin, D. 1964. Theorie dynamique de la diffraction des rayons x par les cristaux deforms. *Bull. Soc. Fr. Miner. Crist.* 87:69.
- Thorkildsen, G. 1987. Three-beam diffraction in a finite perfect crystal. *Acta Crystallogr. A* 43:361-369.
- Tischler, J.Z. and Batterman, B.W. 1986. Determination of phase using multiple-beam effects. *Acta Crystallogr. A* 42:510-514.
- Tolan, M., Konig, G., Brugemann, L., Press, W., Brinkop, F., Kotthaus, J.P. 1992. X-ray diffraction from laterally structured surfaces: total external reflection and grating truncation rods. *Euro. Phys. Lett.* 20:223-228.
- Tolan, M., Press, W., Brinkop, F., Kotthaus, J.P. 1995. X-ray diffraction from laterally structured surfaces: total external reflection. *Phys. Rev. B* 51:2239-2251.
- Vineyard, G.H. 1982. Grazing-incidence diffraction and the distorted-wave approximation for the study of surfaces. *Physical Review B* 26:4146-4159.
- Wang, J., Bedzyk, M.J., and Caffrey, M. 1992. Resonance-enhanced x-rays in thin films: a structure probe for membranes and surface layers. *Science* 258:775.
- Warren, B.E. 1969. *X-ray Diffraction* (Addison Wesley, New York).
- Wechert, E. and Hummer, K. 1997. Multiple-beam x-ray diffraction for physical determination of reflection phases and its applications. *Acta Crystallogr. A* 53:108-143.
- Wechert, E., and Hummer, K. 1997. Multiple-beam x-ray diffraction for physical determination of reflection phases and its applications. *Acta Crystallogr. A* 53:108-143.
- Wechert, E., Schwegle, W., and Hummer, K. 1993. Direct phasing of macromolecular structures by three-beam diffraction. *Proc. R. Soc. Lond. A* 442:33-46.
- Yahnke, C.J., Srajer, G., Haefner, D.R., Mills, D.M., and Assoufid, L. 1994. Germanium x-ray phase plates for the production of circularly polarized x-rays. *Nucl. Instrum. Meth. A* 347:128-133.
- Yoneda, Y. 1963. *Phys. Rev.* 131:2010.
- Zachariasen, W.H. 1945. *Theory of x-ray diffraction in crystals.* John Wiley, New York.
- Zachariasen, W.H. 1965. Multiple diffraction in imperfect crystals. *Acta Crystallogr. A* 18:705-710.
- Zegenhagen, J., Hybertsen, M.S., Freeland, P.E., and Patel, J.R. 1988. Monolayer growth and structure of Ga on Si (111). *Phys. Rev. B* 38:7885.
- Zhang, Y., Colella, R., Shen, Q., and Kycia, S.W. 1997. Dynamical three-beam diffraction in a quasicrystal. In *Proc. 6th International Conf. on Quasicrystals*, Tokyo (Japan).

Key References

- Authier, A., Lagomarsino, S. and Tanner, B.K. 1996. *X-ray and Neutron Dynamical Diffraction: Theory and Applications*, Plenum Press, New York.
- Batterman, B.W. and Cole, H. 1964. Dynamical diffraction of x-rays by perfect crystals. *Rev. Mod. Phys.* 36:681-717.
- Colella, R. 1974. Multiple diffraction of x-rays and the phase problem. computational procedures and comparison with experiment. *Acta Crystallogr. A* 30:413-423.
- Zachariasen, W.H. 1945. *Theory of x-ray diffraction in crystals*. John Wiley, New York.